Geochemistry of the Orhtris Ophiolite, Greece: Evidence for Refertilisation

Barth, M.; Mason, P.R.D.; Davies, G.R.; Dijkstra, A.H.; Drury, M.R.

published in
Journal of Petrology
2003

DOI (link to publisher)
10.1093/petrology/egg058

document version
Publisher's PDF, also known as Version of record

JOURNAL OF PETROLOGY | VOLUME 44 | NUMBER 10 | PAGES 1759–1785 | 2003 | DOI: 10.1093/petrology/egg058

Geochemistry of the Othris Ophiolite, Greece: Evidence for Refertilization?

MATTHIAS G. BARTH[1]*, PAUL R. D. MASON[1], GARETH R. DAVIES[2], ARJAN H. DIJKSTRA[3] AND MARTYN R. DRURY[1]

[1]VENING MEINESZ RESEARCH SCHOOL OF GEODYNAMICS, FACULTEIT AARDWETENSCHAPPEN, UNIVERSITEIT UTRECHT, BUDAPESTLAAN 4, 3584 CD UTRECHT, THE NETHERLANDS

[2]FACULTEIT DER AARD- EN LEVENSWETENSCHAPPEN, VRIJE UNIVERSITEIT AMSTERDAM, DE BOELELAAN 1085, 1081 HV AMSTERDAM, THE NETHERLANDS

[3]DEPARTMENT OF GEOLOGY, UNIVERSITY OF LEICESTER, UNIVERSITY ROAD, LEICESTER LE1 7RH, UK

RECEIVED APRIL 11, 2002; ACCEPTED MARCH 23, 2003

The Othris peridotite massif, Greece, shows conflicting evidence for a mid-ocean ridge and supra-subduction zone tectonic setting with the presence of plagioclase peridotite that may represent an area of either incomplete melt extraction, or melt impregnation and accumulation. To address these problems we focus on a 3 km continuous section in the Fournos Kaïtsa area, consisting of layers of harzburgite, plagioclase harzburgite and plagioclase lherzolite with accurately known structural and petrographic control. Refractory, Cr-rich spinel compositions and light rare earth element depleted clinopyroxenes in the harzburgites are consistent with ~15% dry partial melting. Simple batch and fractional melting models are not sufficient to explain the composition of the residual phases and a multistage model with some melting in the garnet stability field is proposed. The pyroxenes from the plagioclase peridotites have higher Ti and rare earth element contents than those from the harzburgites, but similar refractory spinel compositions in both rock types indicate that the plagioclase peridotites may be products of impregnation of harzburgites with a fractionating melt. These observations are in good agreement with previous structural studies and suggest that the moderately depleted Fournos Kaïtsa mantle section most probably originated at a slow-spreading mid-ocean ridge.

KEY WORDS: *melt impregnation; Othris Ophiolite; plagioclase lherzolite; refertilization*

INTRODUCTION

Mantle peridotites exposed on the Earth's surface provide direct information about processes controlling the geochemical evolution of the upper mantle. Studies of peridotite massifs, such as orogenic lherzolites, are particularly useful because geochemical variations can be determined on scales from micrometres to kilometres and constraints from geological observations can be combined with those based on petrological and geochemical data. The composition of ophiolitic mantle sections, which are thought to be the residua of partial melting, can give information about (1) the nature of the processes responsible for partial melting and melt extraction and (2) the tectono-magmatic environment in which the ophiolites formed.

Potentially, ophiolites can originate in mid-ocean ridge (MOR), back-arc spreading centre, and supra-subduction zone (SSZ) tectonic settings (Miyashiro, 1973; Pearce *et al.*, 1984). The MOR-type ophiolites can be subdivided further into slow-spreading and fast-spreading environments. It is generally assumed that harzburgitic MOR-type mantle sections are formed by high degrees of melt depletion in fast-spreading environments (Niu & Hékinian, 1997; see Moores *et al.*, 2000, for an alternative view). Slow-spreading or continental rift settings are thought to give rise to ophiolites with lherzolitic mantle sections (the lherzolite ophiolite subtype or LOS), corresponding to low degrees of melt depletion (Boudier & Nicolas, 1985; Nicolas, 1986, 1989). Some lherzolite-dominated ophiolites show atypical characteristics when compared with oceanic lithosphere produced at mid-ocean ridges in mature oceans. For example, the Northern Apennine ophiolites consist of older, subcontinental lithospheric

*Corresponding author. Telephone: + 31 30 253 5071. Fax : + 31 30 253 5030. E-mail: barth@post.harvard.edu

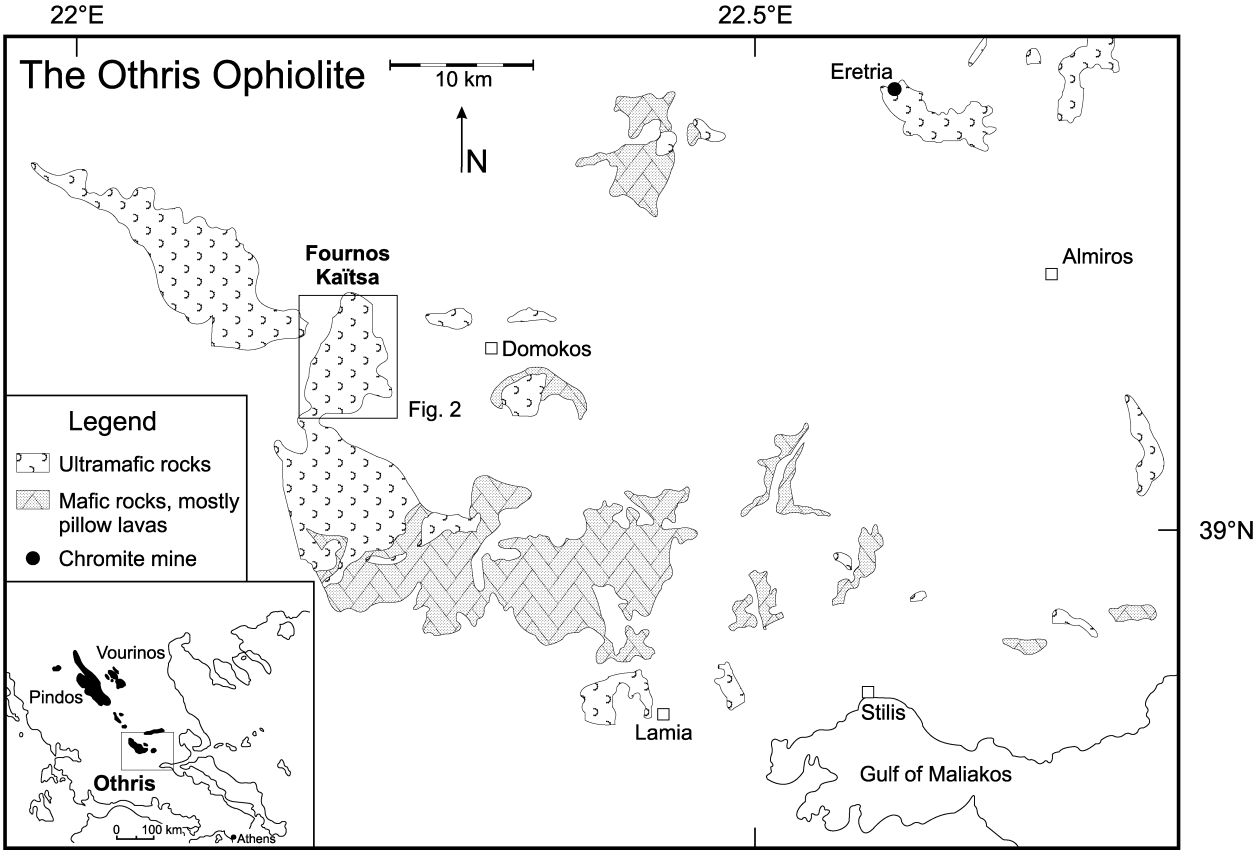

Fig. 1. Simplified geological map of the Othris Ophiolite showing the location of the study area. After Rassios & Konstantopoulou (1993). Inset: location map showing the Othris, Pindos, and Vourinos ophiolites.

mantle, denuded by passive lithosphere extension during the early stages of ocean formation and younger, unrelated mid-ocean ridge basalt (MORB)-type magmatism (Rampone *et al*., 1995; Rampone & Piccardo, 2000).

Distinct types of lherzolite ophiolite are those with voluminous plagioclase lherzolites containing trapped basaltic melts in a peridotite matrix. The occurrence of plagioclase + clinopyroxene blebs and/or veins in some of the plagioclase lherzolites has been variously interpreted as a product of melt segregation or melt impregnation. Those who favour melt segregation argue for *in situ* melts generated during partial melting and incompletely extracted from the host peridotite (Menzies, 1973; Quick, 1981; Takazawa *et al*., 2000). In contrast, melt impregnation involves 'exotic' basaltic melts migrating through depleted lithospheric mantle (Menzies, 1975; Obata & Nagahara, 1987; Rampone *et al*., 1997; Dijkstra *et al*., 2001).

The Othris Ophiolite of central Greece has often been cited as a type example of the LOS (see Nicolas & Dupuy, 1984), as many of the plagioclase lherzolites have bulk-rock compositions similar to those of fertile mantle (Menzies, 1973, 1976; Menzies & Allen, 1974). In contrast, Dijkstra *et al*. (2001) proposed, based on structural and microstructural data, that the plagioclase lherzolites in the Othris peridotite massif were produced by melt impregnation. In this study, we examine the competing hypotheses using mineral major and trace element concentrations from harzburgites and plagioclase peridotites within Othris. The main objectives of this study are: (1) to determine whether the plagioclase lherzolites represent incomplete melt extraction or a region of melt impregnation and accumulation; (2) to resolve the nature of the processes responsible for melt extraction and melt–rock interaction; (3) to constrain the tectonic environment of the Othris Ophiolite.

THE OTHRIS OPHIOLITE

Othris, Pindos, and Vourinos are the three major ophiolite complexes within the Dinaric–Hellenic ophiolite belt of western Greece (Fig. 1). These

ophiolites are interpreted to be remnants of the Neotethys Ocean, which existed between Eurasia and Gondwanaland during the Jurassic and the Cretaceous (Robertson *et al.*, 1991; Stampfli *et al.*, 1998). Structural, trace element, and metallogenic evidence suggests that all three major complexes were once linked together (Smith, 1979; Rassios *et al.*, 1999). Based mainly on the trace element characteristics of the mafic volcanic sequences, these complexes have been interpreted as being formed, entirely or partially, in an island-arc environment (Pearce *et al.*, 1984; Smith & Spray, 1984). The Pindos and Othris complexes are thought to represent more than one tectonic setting as their basalts exhibit both MOR and island-arc affinities (Pearce *et al.*, 1984; Jones & Robertson, 1991).

The dismembered Othris Ophiolite (Fig. 1) is part of the Mirna Group, which is the uppermost tectonic unit of a series of thrust sheets (Smith *et al.*, 1975). These thrust sheets reveal a lateral transition from continental material (clastic sediments and shallow water carbonates) to progressively more pelagic carbonates and finally ophiolites at the top of the stack (Hynes, 1974; Menzies & Allen, 1974; Smith *et al.*, 1975; Smith, 1993). The origin of the Othris Ophiolite remains controversial. It has been variously interpreted as being formed in a relatively slow-spreading environment, near a continental margin at the inception of rifting (Menzies, 1973, 1976; Menzies & Allen, 1974), at a Mid-Atlantic type spreading centre (Rassios & Konstantopoulou, 1993; Dijkstra *et al.*, 2001), or in an island-arc environment (Bizimis *et al.*, 2000; Rassios & Smith, 2001).

Detailed descriptions of all the mantle rock types exposed in the Othris massif, as well as structural maps and cross-sections, have been presented by Dijkstra *et al.* (2001). Our study is focused on a subset of these samples from a 3 km continuous section in the Fournos Kaïtsa area, which consists of layers of harzburgite, plagioclase harzburgite, and plagioclase lherzolite with accurately known stratigraphic control (Fig. 2). Foliations and layering generally strike NW–SE. Fine-grained porphyroclastic harzburgites grade vertically into peridotites with more fertile bulk compositions. Dijkstra *et al.* (2001) interpreted the plagioclase-in boundary as being originally close to horizontal, with the plagioclase peridotites occurring up-section. Upward and eastward from the base of the now tilted section, the peridotites become rich in clinopyroxenite lenses and millimetre-thick veins. At structurally even shallower levels the peridotites become plagioclase bearing. The change from harzburgites to plagioclase peridotites is associated with a change in orientation of the foliation from NW–SE to north–south or NE–SW.

All peridotite samples analysed in this study are characterized by spinel-bearing mantle assemblages showing a complete equilibration in the spinel-facies stability field (with fine- to coarse-grained porphyroclastic textures). The peridotites do not show any petrographic evidence of plagioclase-facies recrystallization such as development of plagioclase and orthopyroxene exsolution in clinopyroxene or plagioclase rims around spinel. Orthopyroxene porphyroclasts in peridotites from the Fournos Kaïtsa area show two distinct morphologies: (1) up to millimetre-size, flaser-like deformed crystals with long, thin, and regular clinopyroxene exsolution lamellae with heavily corroded outlines (Fig. 3a); (2) larger, undeformed crystals with small prismatic or spindle-shaped clinopyroxene exsolution lamellae (Fig. 3b). These undeformed orthopyroxene porphyroclasts often contain blebs of clinopyroxene and/or olivine. The grain boundaries of the orthopyroxene porphyroclasts are irregular because of the presence of many cusp-shaped embayments filled mainly with olivine and in places with clinopyroxene.

Samples 96FK25, 96FK26, GOFOK16A, and GOFOK12 represent the harzburgitic part of the section. Orthopyroxene porphyroclasts are generally <5 mm and are surrounded by rims of fine-grained polyphase material (mainly olivine and orthopyroxene). The orthopyroxene clasts surrounded by fine-grained polyphase rims are embedded into coarser domains of predominantly olivine and minor interstitial orthopyroxene. Samples GOF-14 and 96FK14 are taken from the clinopyroxene-enriched layer but do not contain clinopyroxenite lenses or veins and are texturally similar to the other harzburgites.

Samples 96FK13B, 97GOFOK5, GOF-13, and GOF1 are plagioclase peridotites. No attempt is made to distinguish between plagioclase harzburgites and plagioclase lherzolites. Sample 97GOF21 has a troctolitic composition. The plagioclase peridotites are predominantly fine-grained tectonites, containing orthopyroxene porphyroclasts <5 mm in diameter. Plagioclase occurs as single crystals or in elongated polycrystalline clusters (Fig. 3c and d) and is commonly associated with clinopyroxene and/or orthopyroxene. Generally, plagioclase preserves a magmatic texture in plagioclase clusters and plagioclase crystals contain relatively wide straight twin lamellae (Fig. 3c and d).

ANALYTICAL TECHNIQUES

The major element compositions of olivine, orthopyroxene, clinopyroxene, plagioclase, and spinel were determined by electron microprobe analysis (EMPA) using the Jeol JXA-8600 wavelength-dispersive

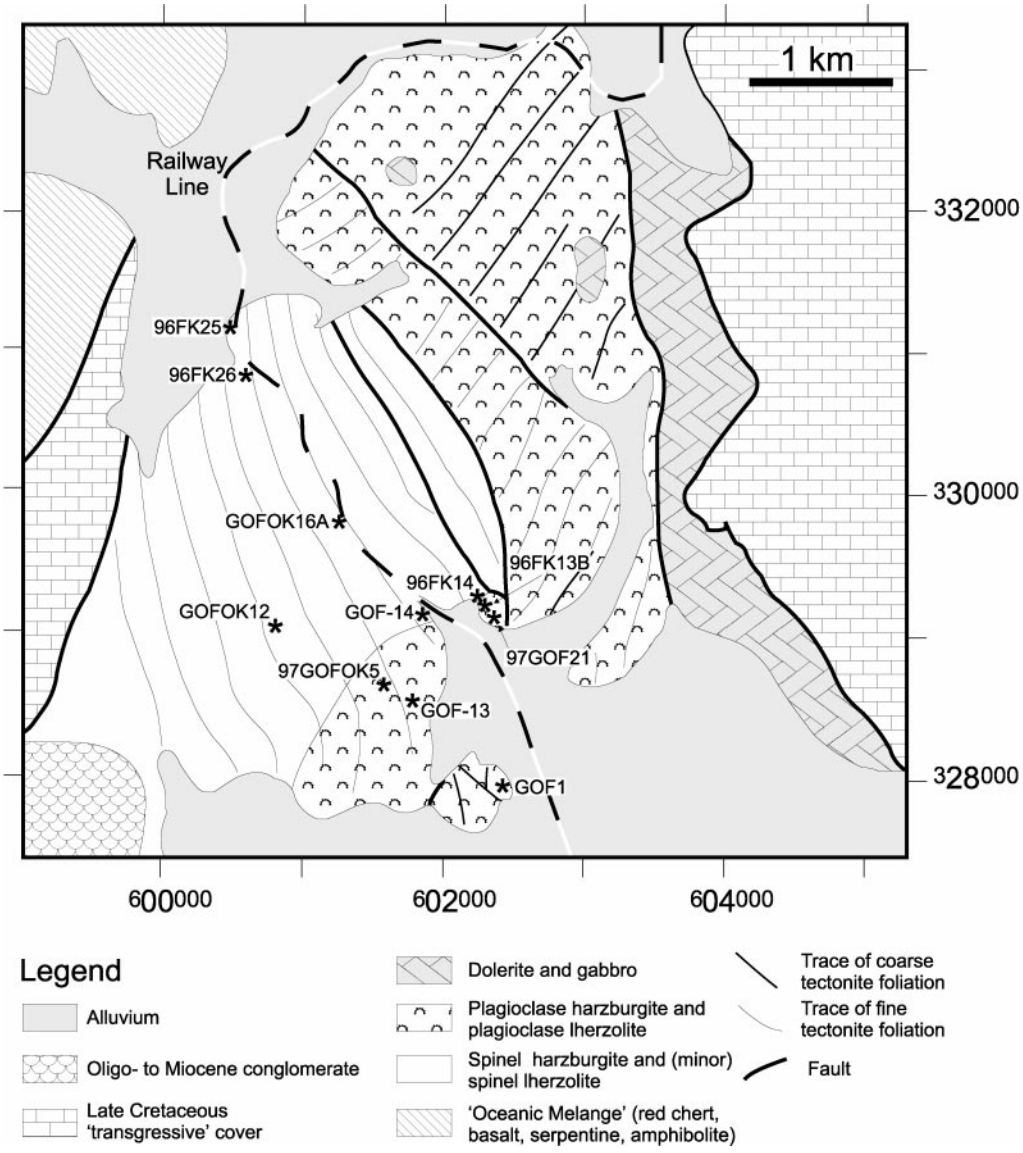

Fig. 2. Structural map of the Fournos Kaïtsa area, showing the transition from plagioclase-free to plagioclase-bearing peridotites and the sample locations. Indicated are orientations of tectonite foliations and lineations, major fault contacts, and the railway line. After Dijkstra *et al.* (2001).

system at the University of Utrecht. An accelerating potential of 15 kV and a beam current of 10 nA were used.

Orthopyroxene, clinopyroxene, and plagioclase were analysed for minor and trace elements by laser ablation–inductively coupled plasma-mass spectrometry (LA–ICP-MS) at the University of Utrecht. Ablation was achieved with a Microlas Geolas 200Q 193 nm Ar–F excimer laser system (Günther *et al.*, 1997), using a pulse repetition rate of 10 Hz and 60–120 μm crater diameters. Analyses were performed on a Micromass Platform inductively coupled plasma-mass spectrometer in pulse counting mode (one point per peak). Data reduction follows the procedures outlined by Longerich *et al.* (1996). The amount of material ablated in laser sampling is different for each spot analysis. Consequently, the detection limits are different for each spot and are calculated for each individual acquisition. ^{43}Ca and ^{30}Si were used as internal standards. Analyses were calibrated against the silicate glass reference material NIST 612 using the values of Pearce *et al.* (1997), and the US Geological Survey (USGS) glass standard BCR-2G was measured to monitor accuracy (see Table 6, below).

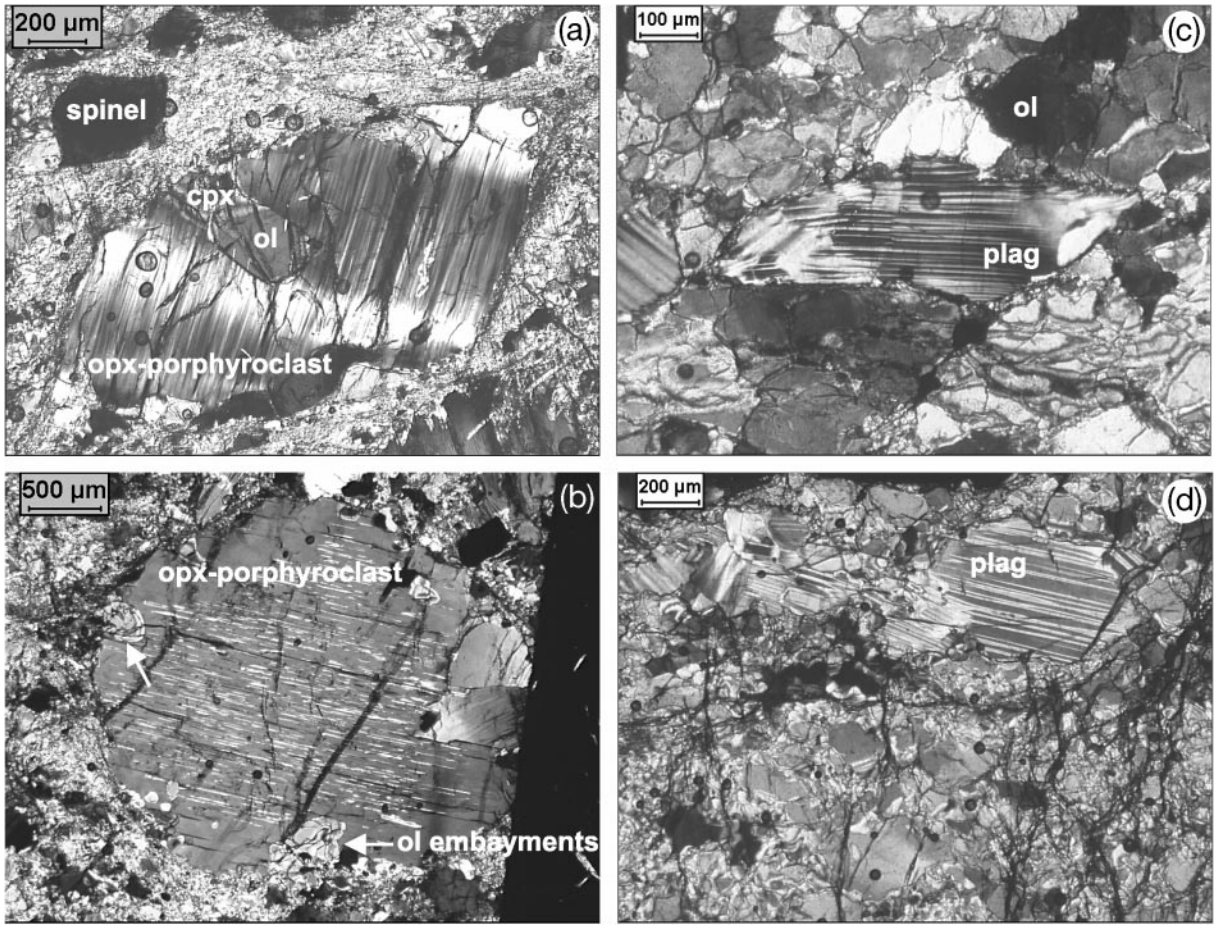

Fig. 3. Photomicrographs in cross-polarized light of Othris peridotites. (a) Deformed orthopyroxene porphyroclast with long, thin, and regular clinopyroxene exsolution lamellae. (b) Undeformed orthopyroxene porphyroclast with shorter, wider, and irregular clinopyroxene exsolution lamellae, with irregular outlines caused by olivine embayments. (c) and (d) Elongated, polycrystalline plagioclase cluster in plagioclase peridotites.

RESULTS

Major element mineral chemistry

The major element compositions of olivine, orthopyroxene, clinopyroxene, plagioclase, and spinel are presented in Tables 1–5. Olivine is homogeneous with Mg-number [100 × Mg/(Mg + Fe)] = 90; only olivine from the troctolite 97GOF21 has a lower Mg-number of 88 (Table 1). Orthopyroxenes in the plagioclase peridotites have lower Mg-number and higher Ti contents (Mg-number = 89–90; 0·07–0·14 wt % TiO_2) than in the harzburgites (Mg-number = 90; TiO_2 ≤0·06 wt %; Table 2). Orthopyroxene is homogeneous with respect to monovalent and divalent cations; no significant compositional difference exists between the deformed and the undeformed porphyroclasts and the fine-grained orthopyroxene. In contrast, Al^{3+} and Cr^{3+} decrease from core to rim of the orthopyroxene porphyroclasts (Fig. 4). Al and Cr contents of the matrix orthopyroxene are lower than or overlap with the rims of the porphyroclasts.

Clinopyroxenes in the plagioclase peridotites have lower Mg-number and higher Na and Ti contents (Mg-number = 91–93; 0·21–0·53 wt % Na_2O; 0·19–0·50 wt % TiO_2) than in the harzburgites (Mg-number = 93; 0·07–0·14 wt % Na_2O; TiO_2 ≤0·15 wt %; Table 3). Large clinopyroxene crystals show similar zoning patterns to the orthopyroxene porphyroclasts, with Al and Cr decreasing from core to rim. Plagioclases in the plagioclase peridotites are anorthite rich ($An_{80–97}$, Table 4) and homogeneous.

Spinel composition is homogeneous within samples (except 97GOFOK5, which has rim compositions with lower Cr-number and higher Mg-number than the interior) but is variable between samples. Cr-number [100 × Cr/(Cr + Al)] ranges from 23 to 47, Mg-number from 53 to 69 (Table 5). Cr-number of spinels from the plagioclase peridotites falls within the range of

Table 1: Major element composition of olivine determined by electron microprobe

Sample:	96FK25		96FK26		GOFOK16A		GOFOK12		GOF-14		96FK14	
Type:	harzburgite		harzburgite		harzburgite		harzburgite		harzburgite		harzburgite	
Spots:	$n = 9$	1σ	$n = 9$	1σ	$n = 9$	1σ	$n = 8$	1σ	$n = 9$	1σ	$n = 9$	1σ
SiO_2	40·77	0·17	40·44	0·14	40·48	0·29	40·91	0·29	40·67	0·08	40·81	0·08
FeO	9·34	0·16	9·65	0·19	9·59	0·13	9·37	0·14	9·12	0·16	9·63	0·19
MnO	0·12	0·01	0·11	0·01	0·13	0·01	0·12	0·01	0·11	0·01	0·13	0·01
NiO	0·40	0·03	0·39	0·03	n.d.	0·42	0·01	0·43	0·03	0·44	0·04	
MgO	49·53	0·17	49·51	0·20	48·57	0·41	49·36	0·27	49·26	0·30	49·09	0·14
Total	100·18		100·12		98·79		100·19		99·62		100·13	
Mg-no.	90·4	0·2	90·1	0·2	90·0	0·2	90·4	0·1	90·6	0·2	90·1	0·2

Sample:	96FK13B		97GOFOK5		GOF-13		97GOF21		GOF1	
Type:	plagioclase peridotite		plagioclase peridotite		plagioclase peridotite		troctolite		plagioclase peridotite	
Spots:	$n = 12$	1σ	$n = 8$	1σ	$n = 10$	1σ	$n = 10$	1σ	$n = 10$	
SiO_2	40·98	0·20	40·86	0·16	40·88	0·11	40·35	0·15	40·57	
FeO	9·29	0·28	9·70	0·16	9·60	0·17	11·45	0·18	9·71	
MnO	0·11	0·01	0·12	0·01	0·11	0·01	0·14	0·02	0·14	
NiO	0·42	0·03	0·41	0·04	0·39	0·03	n.d.		0·39	
MgO	49·42	0·36	49·10	0·23	49·34	0·28	47·18	0·23	48·87	
Total	100·26		100·23		100·36		99·15		99·71	
Mg-no.	90·5	0·3	90·0	0·2	90·2	0·2	88·0	0·2	89·9	

GOF1 from Dijkstra *et al.* (2001). n.d., not determined. TiO_2, Al_2O_3, Cr_2O_3, CaO, and Na_2O were measured but below the detection limit in all samples.

the harzburgites but some samples (GOF1, 97GOF21) are more Fe rich than spinels from plagioclase-free rocks with similar Cr-number (see Dijkstra *et al.*, 2001). There is a positive correlation between spinel and clinopyroxene Ti contents, with the plagioclase peridotites having higher Ti contents (Fig. 5). Similar observations have been made in studies of abyssal peridotites (Dick & Bullen, 1984; Cannat *et al.*, 1990; Seyler & Bonatti, 1997; Tartarotti *et al.*, 2002).

Trace element mineral chemistry

The trace element compositions of orthopyroxene, clinopyroxene, and plagioclase, determined by LA–ICP-MS, are presented in Tables 6–8. All samples show variable degrees of alteration. Therefore, care was taken to perform analyses on crack-free, unaltered areas of the minerals. The combination of the high-quality optical imaging system of the Geolas laser ablation system and the time-resolved analysis of the ablation signals ensures that altered parts of the minerals were recognized and excluded from the trace element analyses.

Orthopyroxenes have light rare earth element (LREE) concentrations below the detection limit (except GOF1). Chondrite-normalized Yb contents (Yb_N) range from 0·4 to 0·9 in the plagioclase-free rocks and from 0·6 to 2·2 in the plagioclase peridotites (Fig. 6). All orthopyroxenes have convex-downward heavy rare earth element (HREE) patterns, with $(Dy/Yb)_N$ from 0·15 to 0·39. These patterns are very different from those for orthopyroxene from a clinopyroxene-free harzburgite from the Eretria submassif of the Othris Ophiolite reported by Bizimis *et al.* (2000), which has a flat REE pattern with $(Dy/Yb)_N = 0·70$ (Fig. 6).

Clinopyroxenes are LREE depleted with Yb_N ranging from 1·6 to 3·7 in the plagioclase-free rocks and from 4·8 to 8·7 in the plagioclase peridotites (Fig. 7). Most clinopyroxenes have relatively flat HREE patterns, with $(Dy/Yb)_N$ from 0·5 to 1·2. These chemical features closely resemble those of clinopyroxenes in abyssal peridotites (Johnson *et al.*, 1990). Some clinopyroxenes show negative Eu anomalies ($Eu/Eu^* = 0·57 – 1·0$) and/or 'spoon-shaped' REE patterns with relative enrichment of La and Ce.

Table 2: Major element composition of orthopyroxene determined by electron microprobe

Sample:	96FK25		96FK26			GOFOK16A			GOFOK12			GOF-14			96FK14		
Type:	harzburgite		harzburgite			harzburgite			harzburgite			harzburgite			harzburgite		
	average		matrix	rims	cores	matrix	rims	cores	matrix	rims	cores	matrix	rims	cores	matrix	rims	cores
Spots:	$n = 9$	1σ	2	7	7	7	5	13	2	4	6	3	4	7	3	9	8
SiO_2	55·24	0·30	56·05	56·13	55·74	56·64	55·97	55·36	56·86	55·11	54·71	56·24	55·64	55·21	56·10	55·65	55·33
TiO_2	0·02	0·01	0·03	0·02	0·03	0·03	0·03	0·03	0·02	0·04	0·04	0·05	0·05	0·07	0·02	0·04	0·04
Al_2O_3	3·38	0·09	1·91	2·03	2·52	1·63	2·54	3·18	2·02	3·57	3·95	2·02	2·50	2·96	2·69	3·19	3·64
Cr_2O_3	0·62	0·05	0·37	0·50	0·64	0·17	0·43	0·63	0·21	0·57	0·68	0·32	0·50	0·62	0·38	0·53	0·69
FeO	6·18	0·04	6·38	6·28	6·23	6·57	6·42	6·36	6·40	6·15	6·20	6·21	6·13	6·11	6·45	6·42	6·41
MnO	0·13	0·01	0·12	0·13	0·13	0·14	0·15	0·14	0·13	0·14	0·13	0·14	0·13	0·13	0·15	0·14	0·14
MgO	33·31	0·14	34·38	34·25	33·71	33·76	33·38	32·95	34·22	33·10	33·22	33·80	33·42	33·06	33·40	33·05	32·96
CaO	0·62	0·13	0·46	0·55	0·63	0·40	0·48	0·64	0·45	0·77	0·53	0·50	0·58	0·65	0·59	0·62	0·67
Total	99·60		99·80	99·98	99·72	99·36	99·41	99·30	100·38	99·56	99·56	99·37	99·04	98·90	99·88	99·72	99·98
Mg-no.	90·6	0·1	90·6	90·7	90·6	90·2	90·3	90·2	90·5	90·6	90·5	90·7	90·7	90·6	90·2	90·2	90·2

Sample:	96FK13B			97GOFOK5			GOF-13			97GOF21			GOF1		
Type:	plagioclase peridotite			plagioclase peridotite			plagioclase peridotite			troctolite			plagioclase peridotite		
	matrix	rims	cores	matrix	rims	cores	matrix	rims	cores	matrix	rims	cores	matrix	rims	cores
Spots:	4	1	11	3	5	6	4	4	9	4	1	4	12	6	34
SiO_2	57·06	56·50	55·51	56·43	56·20	55·36	57·01	55·71	55·47	56·06	55·48	55·55	55·79	56·16	55·46
TiO_2	0·06	0·06	0·07	0·07	0·07	0·09	0·06	0·07	0·08	0·07	0·05	0·08	0·13	0·10	0·14
Al_2O_3	1·60	2·30	3·55	2·19	2·67	3·74	1·86	3·07	3·47	1·94	2·13	2·44	2·37	2·21	3·21
Cr_2O_3	0·21	0·34	0·72	0·25	0·43	0·74	0·23	0·53	0·65	0·31	0·44	0·45	0·40	0·38	0·66
FeO	6·38	6·26	6·24	6·75	6·64	6·39	6·40	6·38	6·37	7·58	7·59	7·41	6·95	7·18	7·07
MnO	0·13	0·15	0·12	0·12	0·14	0·14	0·14	0·14	0·13	0·18	0·18	0·16	0·16	0·15	0·16
MgO	34·19	34·01	33·03	33·58	33·45	32·84	33·87	33·19	33·02	32·76	32·79	32·49	33·66	33·89	33·39
CaO	0·39	0·61	0·75	0·51	0·57	0·63	0·47	0·56	0·69	0·61	0·54	0·65	0·60	0·58	0·60
Total	100·12	100·29	100·09	100·03	100·27	100·01	100·13	99·75	99·97	99·52	99·20	99·26	100·08	100·67	100·70
Mg-no.	90·5	90·6	90·4	89·9	90·0	90·2	90·4	90·3	90·2	88·5	88·5	88·7	89·4	89·20	89·20

GOF1 from Dijkstra *et al.* (2001). n.d., not determined. NiO and Na_2O were measured but below the detection limit in all samples.

Table 3: Major element composition of clinopyroxene determined by electron microprobe

Sample:	96FK25		96FK26			GOFOK16A			GOFOK12		GOF-14		96FK14	
Type:	harzburgite average		harzburgite			harzburgite			harzburgite average		harzburgite average		harzburgite average	
			matrix	rims	cores	matrix	rims	cores						
Spots:	$n = 6$	1σ	6	5	8	8	3	6	$n = 9$	1σ	$n = 9$	1σ	$n = 10$	1σ
SiO_2	52·19	0·62	52·40	52·89	52·22	52·28	52·86	51·66	51·93	0·42	52·09	0·43	52·07	0·39
TiO_2	0·08	0·01	0·05	0·04	0·05	0·12	0·10	0·11	0·11	0·01	0·15	0·03	0·13	0·02
Al_2O_3	3·02	0·56	2·16	1·81	2·51	2·67	2·07	3·54	3·31	0·64	2·66	0·40	3·39	0·45
Cr_2O_3	0·70	0·21	0·81	0·60	0·83	0·70	0·42	0·94	0·73	0·15	0·70	0·13	0·82	0·19
FeO	2·19	0·09	2·12	2·07	2·26	2·11	2·30	2·43	2·40	0·28	2·29	0·21	2·38	0·13
MnO	0·07	0·01	0·06	0·07	0·08	0·08	0·08	0·07	0·08	0·01	0·08	0·03	0·08	0·01
MgO	16·97	0·31	17·18	17·48	17·07	16·66	17·24	16·45	17·09	0·90	16·84	0·29	16·61	0·26
CaO	23·56	0·27	24·00	24·25	23·80	24·09	23·78	23·39	23·09	1·30	23·89	0·31	23·72	0·25
Na_2O	0·07	0·02	0·09	0·07	0·10	0·06	0·05	0·09	0·11	0·03	0·09	0·02	0·14	0·02
Total	98·91		98·92	99·33	98·96	98·77	98·90	98·68	98·90		98·84		99·40	
Mg-no.	93·2	0·3	93·5	93·8	93·1	93·4	93·0	92·3	92·7	0·5	92·9	0·6	92·6	0·4

Sample:	96FK13B		97GOFOK5		GOF-13			97GOF21			GOF1
Type:	plagioclase peridotite average		plagioclase peridotite average		plagioclase peridotite			troctolite			plagioclase peridotite
					matrix	rims	cores	matrix	rims	cores	
Spots:	$n = 10$	1σ	$n = 14$	1σ	2	6	8	1	7	11	in clusters $n = 18$
SiO_2	52·16	0·52	52·33	0·54	53·34	52·47	51·44	52·85	52·42	51·92	51·94
TiO_2	0·20	0·02	0·23	0·03	0·17	0·24	0·21	0·20	0·22	0·28	0·40
Al_2O_3	3·36	0·53	3·41	0·73	1·94	3·08	4·14	2·78	2·96	3·49	3·41
Cr_2O_3	0·87	0·24	0·77	0·21	0·38	0·75	1·05	0·66	0·78	0·96	0·77
FeO	2·30	0·07	2·45	0·16	2·36	2·30	2·43	2·97	2·87	2·91	2·56
MnO	0·07	0·01	0·08	0·02	0·07	0·07	0·08	0·09	0·09	0·10	0·08
MgO	16·59	0·35	16·65	0·45	17·11	16·76	16·07	16·55	16·27	15·94	16·65
CaO	23·44	0·28	23·21	0·50	23·72	23·51	23·16	22·83	22·74	22·65	23·16
Na_2O	0·19	0·02	0·21	0·04	0·15	0·19	0·25	0·49	0·51	0·55	0·40
Total	99·23		99·39		99·29	99·40	98·88	99·42	98·86	98·82	99·38
Mg-no.	92·8	0·2	92·4	0·5	92·8	92·9	92·2	90·9	91·0	90·7	91·8

GOF1 from Dijkstra *et al*. (2001). n.d., not determined. NiO was measured but below the detection limit in all samples.

Clinopyroxene/orthopyroxene partition coefficients ($D^{cpx/opx}$) for REE are similar for all samples analysed and decrease systematically from the middle REE (MREE: $D_{Dy} = 10$–21) to the HREE ($D_{Yb} = 4$–6). Such systematics are typical for high-temperature subsolidus equilibrium partitioning in peridotites (Eggins *et al*., 1998) and indicate that the silicate phases in the Othris peridotites were at, or close to, trace element equilibrium.

REE concentrations in plagioclase are generally low, between 0·03 and 0·5 times chondrite, with strong positive Eu anomalies ($Eu/Eu^* = 12$). Sr is homogeneous between the grains of a given sample but concentrations range from 1 to 78 ppm from one sample to another.

DISCUSSION

Melting and refertilization models

The modelling performed below assumes that the evolution of the peridotites started with a partial melting

Table 4: Major element composition of plagioclase determined by electron microprobe

Sample:	96FK13B		97GOFOK5		GOF-13		97GOF21		GOF1
Type:	plagioclase peridotite		plagioclase peridotite		plagioclase peridotite		troctolite		plagioclase peridotite
Spots:	$n = 12$	1σ	$n = 16$	1σ	$n = 11$	1σ	$n = 10$	1σ	$n = 10$
SiO_2	43·33	0·14	43·23	0·25	43·37	0·28	47·38	0·31	45·3
Al_2O_3	35·98	0·09	35·94	0·13	36·10	0·17	32·95	0·18	34·89
FeO	0·06	0·03	0·11	0·05	0·08	0·05	0·08	0·04	0·12
CaO	19·46	0·16	19·51	0·19	19·51	0·17	16·28	0·22	17·82
Na_2O	0·35	0·06	0·39	0·10	0·36	0·09	2·30	0·11	1·41
Total	99·21		99·20		99·44		99·02		99·60
An	96·8	0·5	96·5	0·9	96·8	0·8	79·7	1·0	86·9

GOF1 from Dijkstra *et al.* (2001). n.d., not determined. TiO_2, Cr_2O_3, MnO, and MgO were measured but below the detection limit in all samples.

event. If the observed compositions are not explicable by a single-stage melting event, a subsequent melt percolation event is also modelled. An incremental, non-modal batch melting model is used, in which melt is extracted at 0·1% increments [non-modal batch melting equations from Shaw (1970); see also Johnson *et al.* (1990)]. The melting process within the spinel stability field leads to exhaustion of clinopyroxene after 25% partial melting. Initial composition, source mineralogy, melting phase proportions, and partition coefficients are given in Table 9. The extent of melting is calculated based on the concentration of moderately incompatible elements in clinopyroxene by using elements (i.e. Ti and HREE) that are the least sensitive to any possible subsequent melt percolation and other possible secondary enrichment processes.

In addition to the melting process within the spinel stability field, a multistage melting model was tested using: (1) variable degrees of near-fractional melting in the garnet stability field using the melting modes and partition coefficients of Walter (1998) and Johnson (1998), respectively; (2) calculation of new modal and REE source abundances following garnet to spinel phase transition using the equation of Johnson *et al.* (1990); (3) continued melting in the spinel stability field using the near-fractional melting model described above.

To model a melt percolation event, the mantle–melt interaction process proposed by Kelemen *et al.* (1990) was used. In this model, ascending liquids from deeper (more fertile) parts of the mantle react with a depleted peridotite at shallower parts of the mantle. A 3% aggregate melt from the MORB source reacts with a lherzolitic residue formed from 15% melting of the same source. The assimilation–fractional crystallization (AFC) equations of DePaolo (1981) were used.

As an alternative to the dry melting model followed by melt percolation, a fluid-induced refertilization–hydrous melting model was assessed following the model proposed by Bizimis *et al.* (2000). Compared with dry melting, hydrous melting causes the proportion of clinopyroxene entering the melt to decrease from 0·72 to 0·56, and the rate of orthopyroxene entering the melt is increased (Table 9). A depleted source, modelled as a MORB source that has undergone 9% dry partial melting, is used as the starting composition. The model assumes that a depleted source becomes hydrated and remelts above a subducting slab and that a constant fluid flux sustains the hydrous melting process. An incremental model is used, in which fluid is added at 0·005 wt % increments and melt is extracted at 0·1% increments, resulting in hydrous melts with 5 wt % H_2O.

Primary features of the plagioclase-free peridotites

To identify the nature of the trapped basaltic melts represented by the plagioclase + clinopyroxene veins and the mechanisms of melt–rock interaction in the plagioclase peridotites, it was first necessary to determine the petrological and compositional characteristics of the plagioclase-free peridotites. Pyroxene porphyroclasts with relatively high Al and Cr and low Si contents in the cores have zoning profiles (Fig. 4) consistent with the core compositions reflecting equilibration within the spinel facies (Takazawa *et al.*, 1996). The lower Al and Cr contents in the rims and matrix pyroxenes probably reflect cooling rather than decompression. The decrease in Cr content is

Table 5: Major element composition of spinel determined by electron microprobe

Sample:	96FK25		96FK26		GOFOK16A		GOFOK12		GOF-14		96FK14	
Type:	harzburgite		harzburgite		harzburgite		harzburgite		harzburgite		harzburgite	
Spots:	$n = 9$	1σ	$n = 9$	1σ	$n = 13$	1σ	$n = 9$	1σ	$n = 9$	1σ	$n = 8$	1σ
TiO_2	0·04	0·01	0·04	0·02	0·05	0·01	0·04	0·01	0·10	0·01	0·05	0·02
Al_2O_3	42·35	1·36	28·73	0·99	43·27	0·82	46·44	1·01	32·47	0·89	45·90	0·50
Cr_2O_3	25·02	1·35	37·95	1·17	22·91	0·64	20·37	1·20	33·68	0·99	20·76	0·53
Fe_2O_3	1·77	0·26	2·50	0·31	3·31	0·36	1·90	0·35	3·62	0·18	2·38	0·26
FeO	12·85	0·29	16·46	0·14	11·92	0·18	12·09	0·14	14·34	0·31	12·26	0·29
MgO	16·60	0·23	12·90	0·16	17·16	0·22	17·43	0·15	14·50	0·25	17·32	0·19
NiO	0·22	0·02	0·12	0·02	n.d.		0·27	0·02	0·15	0·03	0·25	0·03
Total	99·22		99·71		98·80		98·91		99·34		99·30	
Mg-no.	69·7	0·72	58·3	0·49	71·9	0·56	72·0	0·37	64·3	0·87	71·6	0·69
Cr-no.	28·4	1·74	47·0	1·6	26·2	0·9	22·7	1·40	41·0	1·35	23·3	0·62

Sample:	96FK13B		97GOFOK5			GOF-13		97GOF21		GOF1
Type:	plagioclase peridotite		plagioclase peridotite			plagioclase peridotite		troctolite		plagioclase peridotite
			cores		rim					
Spots:	$n = 15$	1σ	$n = 16$	1σ	$n = 1$	$n = 16$	1σ	$n = 8$	1σ	$n = 10$
TiO_2	0·09	0·01	0·08	0·01	0·05	0·10	0·02	0·14	0·02	0·16
Al_2O_3	43·01	0·95	44·70	1·45	48·31	43·67	0·70	35·66	0·71	39·77
Cr_2O_3	24·08	1·19	22·63	1·54	18·69	23·30	0·76	28·79	0·58	25·76
Fe_2O_3	3·14	0·37	2·57	0·53	2·26	3·17	0·33	4·40	0·27	3·58
FeO	12·46	0·41	12·54	0·55	12·10	12·76	0·45	16·71	0·46	15·70
MgO	17·01	0·36	17·11	0·41	17·67	16·88	0·31	13·31	0·34	14·37
NiO	n.d.		n.d.		n.d.			0·16	0·03	0·17
Total	99·87		99·64		99·10	99·91		99·72		99·35
Mg-no.	70·9	1·11	70·9	1·39	72·2	70·2	1·11	58·7	1·27	62·0
Cr-no.	27·3	1·36	25·4	1·88	20·6	26·4	0·91	35·1	0·88	30·3

Fe^{3+} was calculated from the cation sums. GOF1 from Dijkstra *et al.* (2001). n.d., not determined. SiO_2 and ZnO were measured but below the detection limit in all samples.

consistent with the decreased solubility of the Cr–Al component (CrMgTs) in pyroxene as temperature falls:

$$\underset{\text{CrMgTs}}{MgCrAlSiO_6} + \underset{\text{olivine}}{Mg_2SiO_4} = \underset{\text{enstatite}}{Mg_2Si_2O_6} + \underset{\text{spinel}}{MgCrAlO_4} \quad (1)$$

(Nagata *et al.*, 1983). In contrast, the transition from spinel- to plagioclase-facies assemblages results in an anti-correlation between Al and Cr in the pyroxenes, i.e. Al-poor and Cr-rich rims, as Cr cannot be hosted by plagioclase (Rampone *et al.*, 1993). This interpretation, cooling in the spinel facies, is supported by the absence of metamorphic plagioclase in the peridotites of the Fournos Kaïtsa area (Dijkstra *et al.*, 2001). Equilibration within the spinel facies followed by cooling suggests that melting stopped in the spinel stability field ($P > 3$–4 kbar) and, therefore, that the peridotites were formed beneath a relatively thick thermal lithosphere. As the final depth of melting is a function of the spreading rate, the plagioclase-free peridotites probably originated at a slow-spreading ridge (Niu & Hékinian, 1997).

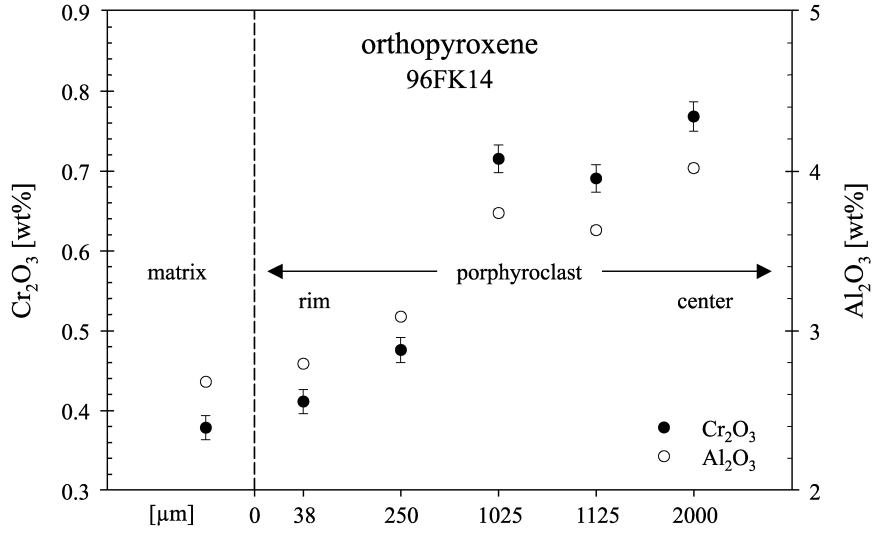

Fig. 4. Comparison of trivalent cation contents (Al_2O_3 and Cr_2O_3) in orthopyroxene matrix neoblast and rim to core zoning in porphyroclasts from a representative harzburgite (96FK14).

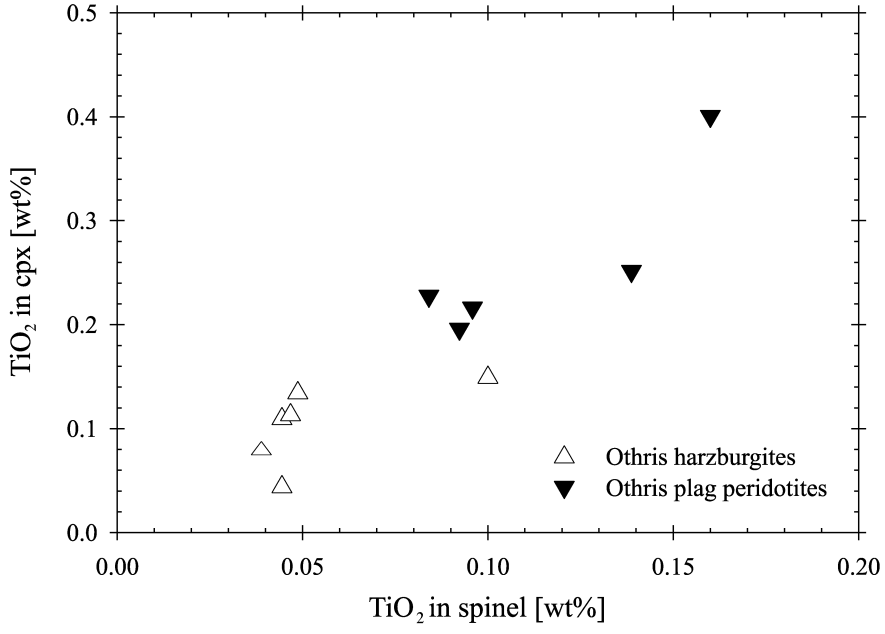

Fig. 5. Correlation diagram of TiO_2 (wt %) in spinel and clinopyroxene.

Equilibration of the plagioclase-free peridotites in the spinel facies allows us to apply Hellebrand *et al.*'s (2001) quantitative melting indicator for residual spinel peridotites based on the Cr-number of spinel. Using Hellebrand *et al.*'s equation

$$F = 10 \ln(\text{Cr-number}) + 24 \quad (2)$$

where F is the degree of melting (in percent), we calculate between 9 and 16% partial melting (12% on average), with the plagioclase peridotites falling within the range of the plagioclase-free peridotites (Fig. 8).

The Ti and Dy contents of the clinopyroxenes from the Othris Ophiolite lie within the field of abyssal peridotites (Fig. 9). The dry spinel peridotite melting model described above predicts the Ti and Dy contents of clinopyroxenes in the Othris Ophiolite and abyssal peridotites reasonably well (Fig. 9). Most of the harzburgites cluster around 15% partial melting; only sample 96FK26 requires higher values (F ~23%). Near-fractional melting in the spinel stability field

Table 6: Trace element composition of orthopyroxene and the USGS reference glass standard BCR-2G determined by LA–ICP-MS

Sample:	96FK25		96FK26		GOFOK16A		GOFOK12		GOF-14		96FK14	
Type:	harzburgite		harzburgite		harzburgite		harzburgite		harzburgite		harzburgite	
Spots:	$n = 8$	1σ	$n = 7$	1σ	$n = 7$	1σ	$n = 5$	1σ	$n = 6$	1σ	$n = 4$	1σ
Cr	5001	469	4300	516	4886	418	6284	631	4535	513	5216	1054
Rb	<0·2		0·08	0·04	<0·14		<0·13		0·06	0·02	0·11	0·02
Sr	0·014	0·012	0·037	0·018	0·018	0·013	0·020	0·008	0·019	0·007	0·030	0·014
Y	0·39	0·08	0·22	0·08	0·54	0·08	0·62	0·12	0·45	0·09	0·62	0·25
Zr	0·027	0·017	0·011	0·006	0·022	0·021	0·061	0·017	0·076	0·016	0·05	0·02
Nb	0·0029	0·0021	<0·005		0·0019	0·0009	<0·02		<0·04		<0·04	
Ba	0·068	0·034	0·023	0·005	<0·03		<0·07		0·061	0·022	<0·2	
La	<0·011		<0·005		<0·004		<0·01		<0·011		<0·02	
Ce	<0·012		<0·010		<0·004		<0·02		<0·009		<0·013	
Pr	<0·005		<0·003		<0·004		<0·007		<0·011		<0·011	
Nd	<0·025		<0·012		<0·012		<0·05		<0·05		<0·05	
Sm	<0·021		<0·021		<0·023		<0·06		<0·08		<0·07	
Eu	<0·008		<0·011		0·0008	0·0001	<0·03		<0·02		<0·02	
Gd	<0·020		<0·013		0·010	0·005	<0·05		<0·08		<0·09	
Dy	0·038	0·020	0·020	0·010	0·050	0·016	0·073	0·033	0·041	0·010	0·060	0·029
Er	0·053	0·013	0·041	0·020	0·080	0·014	0·082	0·017	0·084	0·010	0·082	0·042
Yb	0·122	0·039	0·086	0·042	0·18	0·04	0·156	0·068	0·159	0·049	0·157	0·035
Lu	0·021	0·007	0·016	0·005	0·025	0·007	0·032	0·010	0·031	0·007	0·029	0·008
Hf	0·005	0·000	0·002	0·000	0·0025	0·0019	<0·03		0·019	0·003	<0·04	
Ta	<0·004		<0·002		<0·004		<0·008		<0·011		<0·008	
Pb	0·049	0·020	0·029	0·029	0·018	0·011	0·019	0·015	0·038	0·012	0·052	0·035
Th	0·0006	0·0004	<0·002		<0·002		<0·005		<0·006		<0·006	
U	0·0011	0·0010	<0·002		<0·003		<0·004		<0·004		<0·003	

Sample:	96KF13B		97GOFOK5		GOF-13		97GOF21		GOF-1		BCR-2G	
Type:	plagioclase peridotite		plagioclase peridotite		plagioclase peridotite		troctolite		plagioclase peridotite		Utrecht	
Spots:	$n = 7$	1σ	$n = 7$	1σ	$n = 7$	$n = 4$	1σ	1σ	$n = 1$	1σ	$n = 27$	1σ
Cr	4726	725	4340	653	3627	5216	1054	188	3418	216	20	4
Rb	<0·09		<0·08		<0·17	0·11	0·02		<0·16		45·3	2·5
Sr	0·030	0·009	0·036	0·006	0·010	0·030	0·014	0·003	0·007	0·002	319	14
Y	1·56	0·54	1·71	0·32	1·20	0·62	0·25	0·13	0·76	0·05	31·6	1·6
Zr	0·063	0·028	0·16	0·05	0·11	0·05	0·02	0·03	0·16	0·02	165	13
Nb	<0·014		<0·006		<0·01	<0·04			<0·008		11·2	0·6
Ba	<0·04		<0·03		<0·05	<0·2			0·027	0·010	642	63
La	<0·006		<0·006		<0·007	<0·02			<0·004		24·0	1·3
Ce	<0·009		<0·009		<0·007	<0·013			<0·01		51·0	3·0
Pr	<0·005		<0·004		<0·006	<0·011			<0·004		6·13	0·44
Nd	<0·03		<0·03		<0·02	<0·05			<0·02		25·6	1·4
Sm	<0·04		<0·04		<0·03	<0·07			0·012	0·009	5·86	0·40
Eu	<0·03		0·011	0·006	0·005	<0·02		0·001	0·0027	0·0013	1·68	0·18
Gd	0·074	0·056	0·087	0·038	0·036	<0·09		0·013	0·028	0·009	5·91	0·45

Table 6: Continued

Sample:	96KF13B		97GOFOK5		GOF-13		97GOF21		GOF-1		BCR-2G	
Type:	plagioclase peridotite		plagioclase peridotite		plagioclase peridotite		troctolite		plagioclase peridotite		Utrecht	
Spots:	$n = 7$	1σ	$n = 7$	1σ	$n = 7$	$n = 4$	1σ	1σ	$n = 1$	1σ	$n = 27$	1σ
Dy	0·19	0·08	0·22	0·07	0·12	0·060	0·029	0·02	0·088	0·033	5·75	0·54
Er	0·21	0·05	0·20	0·04	0·17	0·082	0·042	0·02	0·091	0·011	3·13	0·38
Yb	0·33	0·04	0·36	0·05	0·29	0·157	0·035	0·04	0·170	0·038	3·06	0·39
Lu	0·06	0·00	0·059	0·008	0·053	0·029	0·008	0·003	0·044	0·004	0·43	0·07
Hf	0·019	0·01	0·027	0·011	0·018	<0·04		0·006	0·008	0·007	4·08	0·44
Ta	<0·006		<0·005		<0·005	<0·008			<0·002		0·68	0·11
Pb	<0·01		<0·01		<0·02	0·052	0·035		<0·02		21·4	10·3
Th	<0·003		<0·002		<0·005	<0·006			<0·004		5·4	0·4
U	<0·004		<0·002		<0·004	<0·003			<0·002		1·5	0·2

GOF1 from Dijkstra *et al.* (2003). Concentrations are given in ppm (μg/g). n.d., not determined.

cannot reproduce the MREE/HREE fractionation observed in the Othris peridotites. MREE to HREE patterns of the clinopyroxenes are steeper than the flat patterns produced by the single-stage melting model. Johnson *et al.* (1990) showed that up to 10% partial melting in the garnet stability field is required to explain the REE content of some abyssal peridotites. The results of the multistage melting model described above are shown in Fig. 10. The figure indicates that the clinopyroxenes have undergone an integrated 16% partial melting including ~4% melting in the garnet stability field followed by 12% in the spinel stability field (except 96FK26, 24% total melting with 20% in the spinel stability field). Initiation of partial melting in the garnet stability field could also explain why the degree of partial melting derived from the clinopyroxene trace element compositions of the plagioclase-free peridotites is slightly higher than that calculated from the coexisting spinel major element compositions (15% vs 12%). Partial melting in the garnet stability field is recorded by the clinopyroxene trace element composition but not by the spinel composition; the spinel compositions apparently record only the later melting stage in the spinel stability field.

Based on whole-rock major element compositions, it has been suggested that abyssal peridotites cannot be formed solely as residua from fractional or near-fractional melting (Elthon, 1992; Niu *et al.*, 1997; Asimow, 1999; Baker & Beckett, 1999). Such melting models produce residua that contain much too little TiO_2 and Na_2O at a given MgO content and fail to reproduce the required and relatively low SiO_2 and high FeO. Clinopyroxene compositions are also inconsistent with solely near-fractional melting. Near-fractional melting yields residual clinopyroxenes characterized by too low Na_2O at a given Ti content for clinopyroxenes both from abyssal peridotites and from peridotites from the Fournos Kaïtsa area (Fig. 11). Batch melting appears to produce a better fit (Fig. 11), in agreement with the whole-rock data of abyssal peridotites [see review by Asimow (1999)].

These observations show that the composition of the Othris harzburgites cannot be explained by single-stage melting models with constant melting mechanisms. Hybrid models that include both episodes of batch and fractional melting may reconcile the major and trace element compositions of abyssal peridotites (Kelemen *et al.*, 1997; Asimow, 1999) and the Othris peridotites. It is difficult, however, to distinguish the order or relative amounts of batch and fractional melting. It should be noted that, in steady state, one-dimensional, polybaric batch melting models produce residua identical to those generated by equilibrium porous flow (Asimow & Stolper, 1999).

The Othris peridotites show microstructural evidence for the incongruent melting reaction of the pyroxenes to produce olivine and melt that occurs during melting in the spinel stability field (see Table 9). That is, orthopyroxene porphyroclasts often have strongly irregular outlines, with embayments filled with olivine and sometimes clinopyroxene. In addition, small irregular, interstitial orthopyroxene crystals are found between olivine crystals in the olivine-rich domains (Fig. 3b; see also Dijkstra *et al.*, 2002). The replacement of orthopyroxene by olivine and the crystallization of orthopyroxene and/or clinopyroxene is characteristic for decompression melting beneath ocean ridges (e.g. Niu, 1997) and can be

Table 7: Trace element composition of clinopyroxene determined by LA–ICP-MS

Sample:	96FK25		96FK26		GOFOK16A		GOFOK12		GOF-14		96FK14	
Type:	harzburgite		harzburgite		harzburgite		harzburgite		harzburgite		harzburgite	
Spots:	$n = 9$	1σ	$n = 7$	1σ	$n = 7$	1σ	$n = 9$	1σ	$n = 7$	1σ	$n = 7$	1σ
Cr	6425	1718	6513	1582	7721	703	6063	1098	5196	489	6652	1767
Rb	0·58	0·21	0·08	0·07	<0·2		0·29	0·06	0·09	0·04	0·11	0·03
Sr	0·29	0·18	0·479	0·100	0·13	0·05	0·65	0·18	0·19	0·03	0·35	0·15
Y	4·93	1·12	1·90	0·32	5·33	0·74	5·86	0·52	4·07	0·32	5·46	0·65
Zr	0·084	0·057	0·056	0·046	0·039	0·014	0·16	0·10	0·25	0·05	0·15	0·07
Nb	<0·03		0·005	0·003	<0·02		0·068	0·012	<0·05		0·02	0·00
Ba	0·20	0·13	<0·04		0·057	0·075	0·33	0·30	<0·04		0·12	0·00
La	<0·02		0·008	0·003	<0·01		0·027	0·005	<0·02		<0·04	
Ce	<0·03		0·010	0·010	<0·01		0·069	0·033	<0·02		<0·03	
Pr	0·0038	0·0011	0·0011	0·0011	<0·007		0·015	0·010	<0·012		<0·03	
Nd	0·042	0·023	0·025	0·026	0·022	0·012	0·14	0·09	0·049	0·024	0·07	0·02
Sm	0·063	0·032	0·029	0·024	0·082	0·022	0·12	0·07	0·08	0·03	0·20	0·11
Eu	0·023	0·008	0·008	0·003	0·046	0·007	0·061	0·019	0·039	0·018	0·059	0·020
Gd	0·21	0·15	0·057	0·026	0·34	0·07	0·38	0·11	0·32	0·08	0·39	0·16
Dy	0·79	0·17	0·250	0·089	0·80	0·13	0·78	0·15	0·68	0·12	0·84	0·16
Er	0·65	0·17	0·251	0·052	0·63	0·11	0·66	0·16	0·46	0·05	0·56	0·10
Yb	0·75	0·27	0·33	0·09	0·70	0·11	0·77	0·21	0·50	0·11	0·72	0·15
Lu	0·106	0·030	0·047	0·016	0·088	0·018	0·10	0·03	0·062	0·005	0·081	0·013
Hf	0·047	0·030	0·006	0·006	0·021	0·013	0·052	0·021	0·044	0·015	0·060	0·035
Ta	0·009	0·006	<0·003		0·002	0·001	<0·02		<0·02		<0·03	
Pb	0·041	0·027	0·057	0·021	0·019	0·014	0·053	0·021	0·037	0·022	0·029	0·015
Th	<0·005		0·0009	0·0005	<0·004		<0·012		<0·009		<0·013	
U	<0·005		0·0014	0·0016	<0·004		<0·01		<0·006		<0·015	

Sample:	96KF13B		97GOFOK5		GOF-13		97GOF21		GOF-1	
Type:	plagioclase peridotite		plagioclase peridotite		plagioclase peridotite		troctolite		plagioclase peridotite	
Spots:	$n = 8$	1σ	$n = 7$	1σ	$n = 7$	1σ	$n = 7$	1σ	$n = 20$	1σ
Cr	7393	522	5748	584	6728	350	7654	740	n.d.	
Rb	<0·4		<0·3		0·14	0·02	0·08	0·02	0·35	0·16
Sr	0·05	0·01	0·54	0·06	0·37	0·06	2·70	0·16	0·51	0·19
Y	12·3	0·8	12·8	0·6	13·1	0·2	9·95	0·38	18·39	2·59
Zr	0·46	0·06	1·12	0·09	1·09	0·07	2·67	0·32	8·95	1·19
Nb	<0·04		<0·04		0·017	0·01	0·016	0·004	0·030	0·021
Ba	<0·08		<0·11		<0·08		0·033	0·036	0·30	0·21
La	<0·015		0·05	0·01	0·13	0·02	0·10	0·03	0·026	0·014
Ce	0·020	0·008	0·14	0·02	0·28	0·02	0·43	0·05	0·36	0·08
Pr	0·008	0·002	0·034	0·002	0·038	0·006	0·10	0·02	0·18	0·05
Nd	0·18	0·02	0·40	0·07	0·35	0·03	0·83	0·11	1·79	0·30
Sm	0·36	0·03	0·51	0·08	0·44	0·05	0·64	0·07	1·33	0·28
Eu	0·16	0·018	0·20	0·03	0·21	0·03	0·29	0·02	0·48	0·11
Gd	1·05	0·09	1·24	0·11	1·19	0·08	1·17	0·11	2·18	0·30
Dy	2·07	0·14	2·15	0·14	2·20	0·13	1·73	0·10	3·25	0·48

Sample:	96KF13B		97GOFOK5		GOF-13		97GOF21		GOF-1	
Type:	plagioclase peridotite		plagioclase peridotite		plagioclase peridotite		troctolite		plagioclase peridotite	
Spots:	$n = 8$	1σ	$n = 7$	1σ	$n = 7$	1σ	$n = 7$	1σ	$n = 20$	1σ
Er	1·42	0·12	1·42	0·09	1·45	0·04	1·05	0·06	2·01	0·29
Yb	1·33	0·11	1·32	0·10	1·35	0·09	1·01	0·08	1·82	0·28
Lu	0·18	0·012	0·19	0·02	0·18	0·01	0·12	0·01	0·24	0·05
Hf	0·123	0·017	0·14	0·03	0·14	0·02	0·168	0·042	0·61	0·12
Ta	0·0029	0·0004	<0·014		0·006	0·002	0·005	0·002	0·0080	0·0046
Pb	0·008	0·003	<0·06		0·012	0·010	0·031	0·010	0·090	0·066
Th	0·0011	0·0001	<0·008		0·007	0·003	0·022	0·010	0·013	0·010
U	0·0013	0·0005	<0·006		0·002	0·001	0·006	0·002	0·047	0·120

GOF1 from Dijkstra *et al.* (2003). Concentrations are given in ppm (μg/g). n.d., not determined.

Table 8: Trace element composition of plagioclase determined by LA–ICP-MS

Sample:	96KF13B		97GOFOK5		GOF-13		97GOF21		GOF-1	
Type:	plagioclase peridotite		plagioclase peridotite		plagioclase peridotite		troctolite		plagioclase peridotite	
Spots:	$n = 2$	1σ	$n = 4$	1σ	$n = 6$	1σ	$n = 6$	1σ	$n = 7$	1σ
Cr	<3		<5		3·65	0·64	0·78	0·72	n.d.	
Rb	<1		<1		<1·4		0·11	0·04	0·37	0·14
Sr	0·96	0·07	12·6	0·1	7·9	0·4	78·2	3·6	7·19	0·23
Y	<0·2		<0·15		<0·2		0·086	0·017	0·13	0·04
Zr	<0·2		<0·2		<0·2		0·02	0·02	0·07	0·07
Nb	<0·2		<0·16		<0·2		<0·02		0·038	
Ba	<0·8		1·30	0·22	1·67	1·45	3·21	0·58	1·34	0·20
La	<0·1		<0·07		0·07	0·03	0·15	0·05	0·028	0·012
Ce	<0·1		<0·06		0·09	0·07	0·20	0·04	0·18	0·04
Pr	<0·1		<0·06		<0·05		0·026	0·002	0·041	0·017
Nd	<0·2		<0·2		0·08	0·03	0·11	0·05	0·20	0·08
Sm	<0·4		<0·4		0·13	0·08	0·042	0·018	0·090	0·087
Eu	<0·2		0·12	0·03	0·14	0·09	0·14	0·03	0·28	0·06
Gd	<0·4		<0·4		<0·4		0·03	0·02	0·052	0·033
Dy	<0·2		<0·2		<0·2		0·03	0·02	0·043	0·018
Er	<0·2		<0·2		<0·2		<0·025		0·011	0·004
Yb	<0·2		<0·3		0·06	0·01	0·010	0·007	0·020	0·018
Lu	<0·2		<0·07		<0·07		<0·008		0·003	
Hf	<0·3		<0·2		<0·23		0·015	0·012	0·012	0·010
Ta	<0·08		<0·08		<0·07		<0·01		0·005	
Pb	<0·1		<0·12		0·15	0·11	0·12	0·05	0·092	0·023
Th	<0·04		<0·04		<0·05		<0·006		0·003	0·001
U	<0·04		<0·04		<0·04		0·028	0·003	0·009	0·006

GOF1 from Dijkstra *et al.* (2003). Concentrations are given in ppm (μg/g). n.d., not determined.

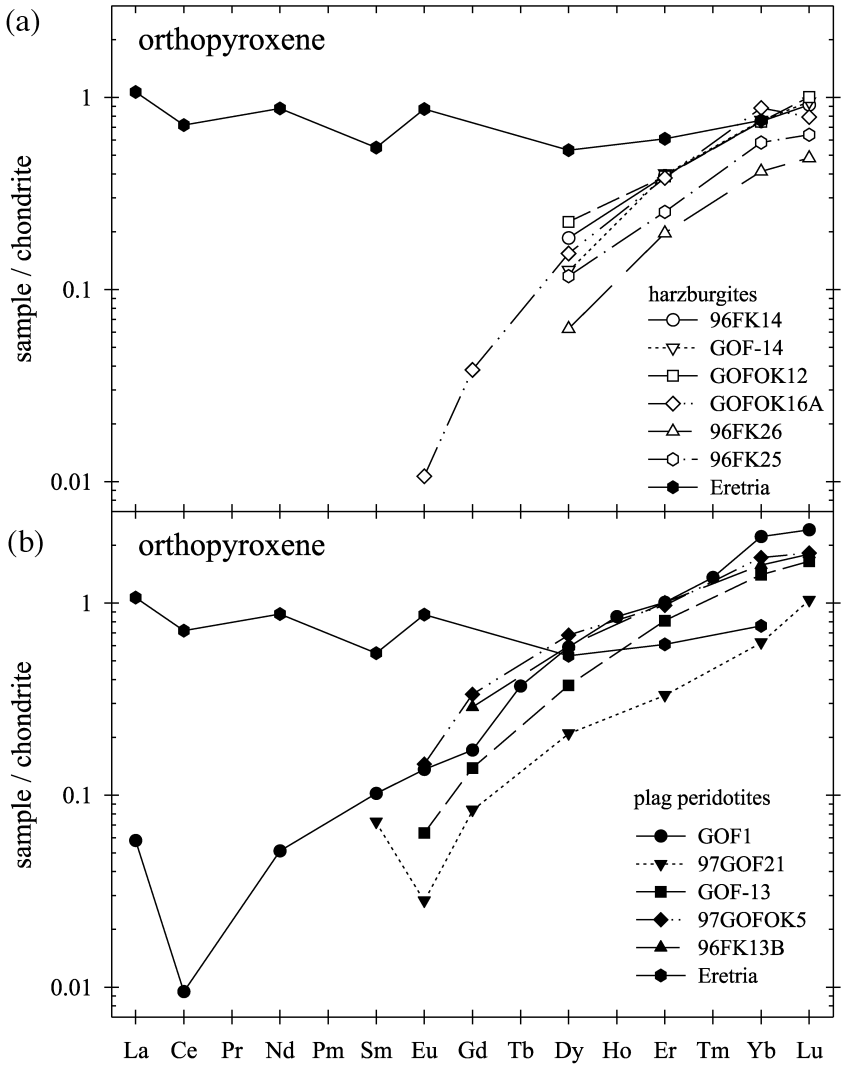

Fig. 6. Chondrite-normalized rare earth element diagram for orthopyroxene from the Fournos Kaïtsa area and Eretria, Othris, Greece. (a) Harzburgites. (b) Plagioclase peridotites. The Eretria analysis (filled hexagons) is from Bizimis *et al.* (2000). Element abundances are normalized to chondrite values of Boynton (1984).

enhanced by the reaction between ascending melts and upwelling peridotite in a melting column. In such an environment, conductive cooling is minimal at depth and melt and peridotite rise adiabatically. Melt rising adiabatically is above its liquidus temperature and thus the melt initially dissolves any peridotite it comes into contact with. This leads to olivine saturation in the melt, which will crystallize olivine and continue to dissolve pyroxene (Kelemen *et al.*, 1992, 1995*a*, 1995*b*). At lower pressure, as both the peridotites and melt pass into a conductive thermal regime, the cooled migrating melt crystallizes first olivine, then olivine + orthopyroxene, and finally clinopyroxene (Kelemen *et al.*, 1992, 1995*b*). In contrast, closed-system crystallization of a trapped melt forms plagioclase, plus olivine and/or orthopyroxene as well as clinopyroxene (Kelemen *et al.*, 1995*a*). The absence of plagioclase in the Othris harzburgites implies open-system crystallization, where the fractionated melt is extracted from the solid.

Incremental non-modal batch melting models successfully predict the shape of the MREE to HREE section of the clinopyroxene REE pattern (Fig. 10). The LREE contents of clinopyroxenes from the spinel harzburgites are not very well defined (Ce_N = 0·01–0·09), because of poor counting statistics at these low concentrations. These values are, however, relatively high and are consistent with a process of porous flow melt–rock interaction. Near-fractional melting yields residua with smooth depleted REE patterns and much lower LREE contents (Fig. 10). Abrupt changes of slope in the LREE end of the patterns (Fig. 10)

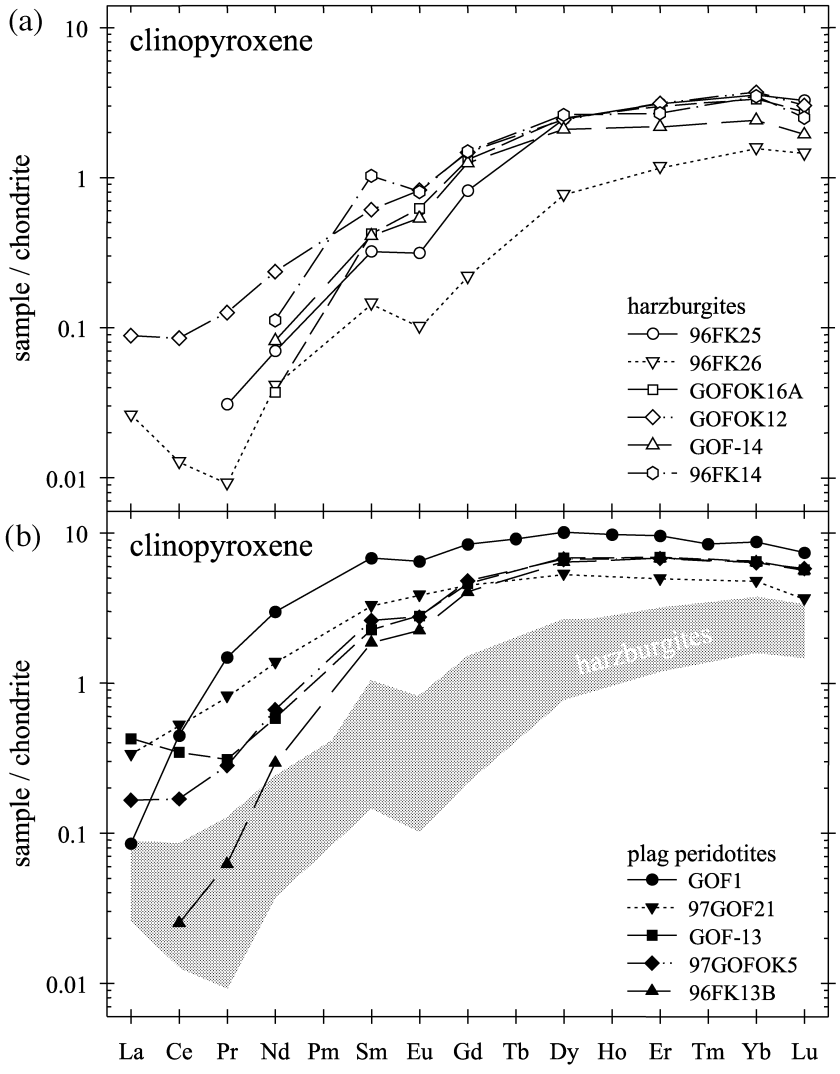

Fig. 7. Chondrite-normalized rare earth element diagram for clinopyroxene from the Fournos Kaïtsa area, Othris, Greece. (a) Harzburgites. (b) Plagioclase peridotites. Grey shaded field shows the compositional range of the harzburgites. Normalized as in Fig. 6.

probably reflect chromatographic effects resulting from melt percolation through a porous peridotite matrix (Navon & Stolper, 1987; Takazawa *et al.*, 1992). These patterns can be matched by mantle–melt interaction with high rock/melt ratios of 1000–10 000 (Fig. 12). Such high rock/melt ratios do not affect the Ti and HREE contents used to constrain the initial depletion of the Othris peridotites. The Othris peridotites are therefore interpreted to have initially evolved as residua from partial melting that later interacted with a limited volume of LREE-enriched melt (or fluid). The abrupt changes of slope in clinopyroxene recorded by the LREE section of the REE pattern develop because effectively La and Ce migrate faster in a melting column than heavier, more compatible REE (Navon & Stolper, 1987; Bodinier *et al.*, 1990). Clinopyroxene REE patterns from the Fournos Kaïtsa area resemble REE patterns from the lowermost mantle section of the Bay of Islands ophiolite (Newfoundland, Canada), which were replicated using a 600–1000 m long melting column, with 1% residual porosity, 5–10 cm/year percolation velocity and short percolation times (Batanova *et al.*, 1998). These parameters result in high rock/melt ratios, qualitatively similar to the conclusions from our AFC model.

The refertilization–hydrous melting model of Bizimis *et al.* (2000) also is able to reproduce the REE concentrations of the Othris peridotites (Fig. 12). Fluid addition buffers the concentration of (fluid-mobile) incompatible trace in the residue and may have caused the enrichment of La and Ce in the Othris peridotites.

Table 9: Partition coefficients, initial mineralogy, melting proportions, MORB source and fluid composition in ppm (μg/g)

	olivine	opx	cpx	spinel	garnet	MORB source	fluid minimum	fluid maximum
Ti	0·007	0·12	0·3	0·07	0·29	927	0	436
Zr	0·003	0·05	0·12	0·04	0·27	6·195	16	365
Sr	0·01	0·04	0·06	0·0006	0·0025	12·93	150	1930
La	0·000007	0·0005	0·0536	0·0006	0·0016	0·161	0·62	18·6
Ce	0·00001	0·0009	0·09	0·0006	0·005	0·5376	1·6	48
Pr	0·00003	0·004	0·13	0·0007	0·018	0·108	0·23	5·88
Nd	0·00007	0·009	0·17	0·0008	0·052	0·7375	1·1	22·2
Sm	0·0007	0·02	0·29	0·0008	0·25	0·304	0·3	4·9
Eu	0·001	0·03	0·35	0·0009	0·4	0·118	0·15	2·85
Gd	0·0012	0·04	0·4	0·0009	0·8	0·417	0·26	3·46
Dy	0·004	0·07	0·45	0·0015	2·2	0·559	0	0·5
Er	0·01	0·07	0·47	0·003	3·6	0·381	0	0·3
Yb	0·005	0·08	0·49	0·0015	6·6	0·392	0	0·3
Na	0·001	0·01	0·1	0·001	0·036	0·2 wt %		
Xa	0·55	0·25	0·18	0·02				
Pa dry	−0·20	0·43	0·72	0·05				
Pa hydrous	−0·10	0·52	0·56	0·02				
Xa	0·57	0·21	0·16		0·06			
Pa dry	0·08	−0·19	0·81		0·30			

Partition coefficients from Kelemen *et al*. (1993) and Johnson (1998). Xa, mineralogy of the MORB source (Johnson *et al*., 1990). Pa dry, melting mode for dry melting. Spinel melting modes from Baker & Stolper (1994); garnet peridotite melt modes from Walter (1998). Pa hydrous, melting mode for hydrous melting in an island-arc environment from Bizimis *et al*. (2000). Compositional range for the fluid component from Bizimis *et al*. (2000).

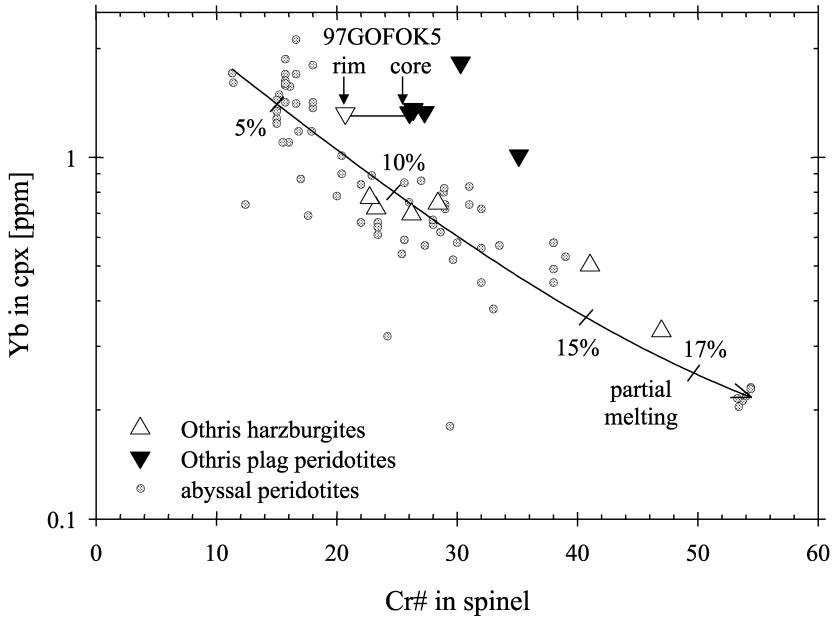

Fig. 8. Diagram of Cr-number in spinel vs Yb (in ppm) in clinopyroxene from Othris peridotites compared with abyssal spinel peridotites. Data sources: Dick & Bullen (1984); Johnson *et al*. (1990); Johnson & Dick (1992); Dick & Natland (1996); Ross & Elthon (1997). Partial melting trend of changing spinel compositions with degree of partial melting of a spinel peridotite from Hellebrand *et al*. (2001). Numbers along the line are percent melting.

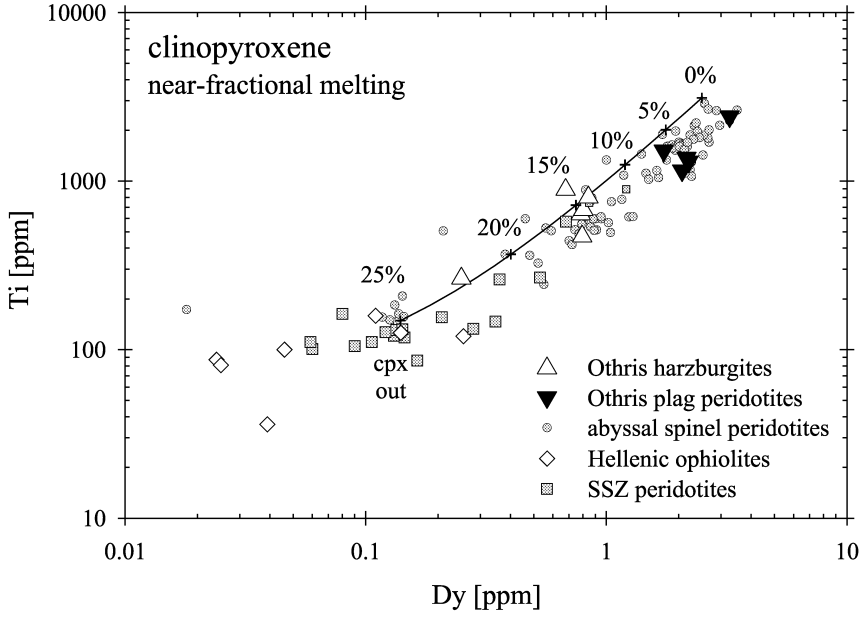

Fig. 9. Diagram of Dy vs Ti (in ppm) in clinopyroxene. Data sources as in Fig. 8 plus Bizimis *et al.* (2000) for Hellenic ophiolites, and Parkinson *et al.* (1992) and Batanova *et al.* (1994) for supra-subduction zone (SSZ) peridotites. Partial melting trend shows residual clinopyroxene compositions during anhydrous melting (incremental batch melting at 0·1% increments) of a MORB source (see text for details). Numbers along the line are percent melting.

The products of dry melting followed by melt percolation and refertilization–hydrous melting are clearly distinguishable at high degrees of partial melting. Unfortunately, however, these processes produce similar Ti, Zr, and REE concentrations at moderate degrees of partial melting (Figs 12 and 13). At high degrees of partial melting, hydrous melting results in much lower Ti and HREE concentrations than dry melting (Fig. 13). Therefore the Othris harzburgites are compatible with a hydrous melting model but do not require one, and additional constraints are required to assess the possible role of hydrous fluids.

Conventionally the ratio of highly incompatible fluid-mobile to fluid-immobile trace elements (e.g. Ba/Nb) could be used to distinguish between the dry and fluid-addition scenarios, but these elements are below or very close to the detection limit. Low Sr/Nd and LREE/Nb ratios (Table 7) in the Othris peridotites, however, give no indication of a subduction-related environment and strongly suggest a MOR setting.

The plagioclase peridotites

The plagioclase peridotites show textural and chemical evidence of melt relics. Plagioclase ± clinopyroxene ± orthopyroxene lenses clearly crystallized from a melt (Menzies, 1973; Dijkstra *et al.*, 2001). The spinel compositions in the plagioclase peridotites provide strong constraints for models of plagioclase peridotite origin. Spinel in the plagioclase peridotites has Cr-number within the range of the plagioclase-free peridotites but the plagioclase peridotites plot off the partial melting trend defined by abyssal peridotites in a diagram of the Cr-number in spinel vs Yb in clinopyroxene (Fig. 8). The plagioclase peridotites have higher Yb contents in clinopyroxene for a given Cr-number than the plagioclase-free peridotites and abyssal peridotites. The plagioclase peridotites are best explained by a two-stage process of initial depletion during partial melting, resulting in the formation of Cr-rich spinel, followed by melt impregnation and crystallization of plagioclase + clinopyroxene. This interpretation is supported by the higher TiO_2 contents of the plagioclase peridotites compared with the harzburgites (Fig. 5), which reflects addition of TiO_2 by significant volumes of impregnating melt (e.g. Cannat *et al.*, 1990).

Spinel shows incomplete chemical equilibration with the impregnating melt. This conclusion is demonstrated by spinel in sample 97GOFOK5, which has rim compositions with lower Cr-number and higher Mg-number than the interior (Table 5). Equilibration with more Fe-rich silicate melts shifts spinel compositions of two samples (GOF1, 97GOF21; Table 5; see also Fig. 8c of Dijkstra *et al.*, 2001) towards lower Mg-number (Dick & Bullen, 1984; Barnes & Roeder, 2001). The preserved spinels have (at least partially) high Cr-number, as a result of lower kinetic barriers for divalent cation exchange than for trivalent cation exchange in spinel (Roeder *et al.*,

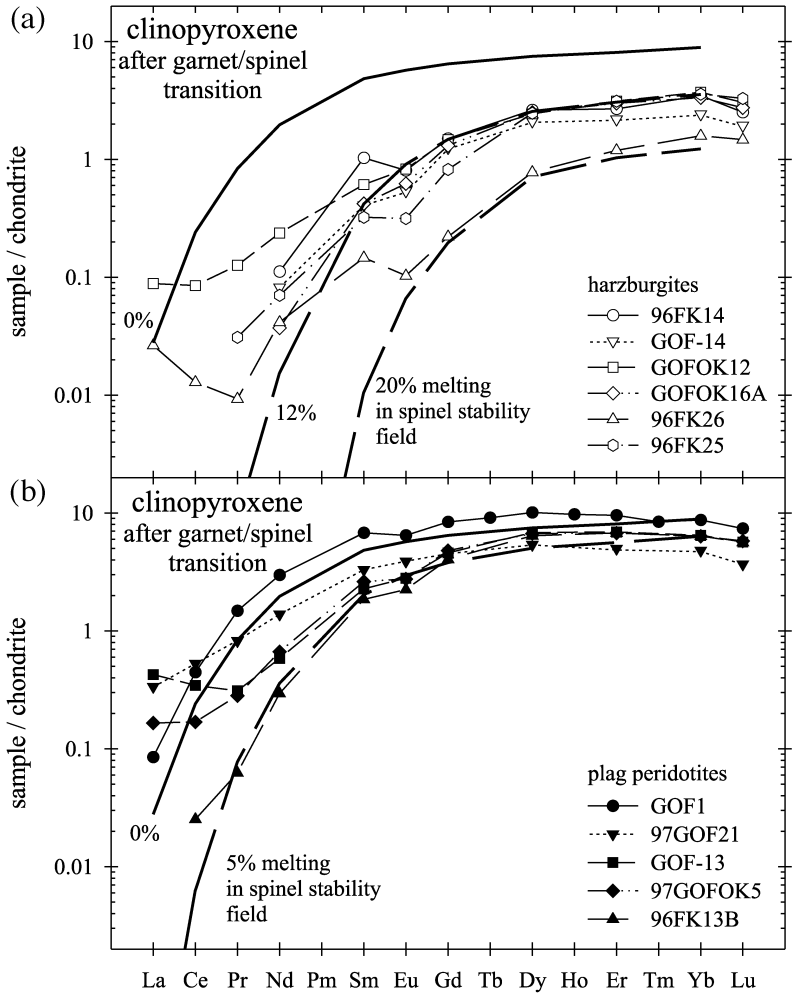

Fig. 10. Chondrite-normalized rare earth element diagram for clinopyroxene from the Fournos Kaïtsa area, Othris, Greece. (a) Harzburgites. (b) Plagioclase peridotites. Also shown are the results obtained for a melting model including 4% of near-fractional melting (incremental batch melting at 0·1% increments) in the garnet stability field followed by various degrees (0%, 5%, 12%, and 20%) of near-fractional melting in the spinel stability field. After 4% of partial melting in the garnet stability field, a new source modal mineralogy and clinopyroxene REE concentrations were calculated to account for the subsolidus garnet to spinel phase transition (see text for details). Normalized as in Fig. 6.

1979; Engi & Evans, 1980). Menzies (1975), however, reported lower Cr-number (~20) in Othris plagioclase peridotites than in harzburgites (Cr-number 30–50), which he interpreted as being caused by reaction with a migrating aluminous melt. These Al-rich spinel compositions were not observed in this study (except in Al-rich rims of sample 97GOFOK5). The preservation of obvious disequilibrium between spinel and silicates indicates that the ambient temperature of the peridotite massif during and following the melt–rock interaction must have been low to prevent extensive diffusional re-equilibration. This is consistent with the observation that plagioclase crystals are often less deformed than olivine in the host peridotite, indicating that melt impregnation and plagioclase crystallization occurred when the mantle section was already conductively cooling, i.e. in a lithospheric thermal regime (Dijkstra *et al.*, 2001).

Mineral compositions of the Othris plagioclase peridotites fall within the depleted end of the field of MOR cumulates (Ross & Elthon, 1993; Dijkstra *et al.*, 2001) but are not as refractory as cumulate minerals from SSZ ophiolites. Olivine in the Othris plagioclase peridotites has Mg-number 88–91, falling within the range of xenocrysts in MORB (Donaldson & Brown, 1977), whereas cumulate olivine in SSZ ophiolites has Mg-number up to 93 (Duncan & Green, 1987, and references therein). Plagioclases in the plagioclase peridotites are more anorthite rich ($An_{80–97}$, Table 4) than typical phenocrystic plagioclase in MORB ($An_{60–85}$). Subsolidus diffusion and equilibration with the peridotite matrix may have modified the

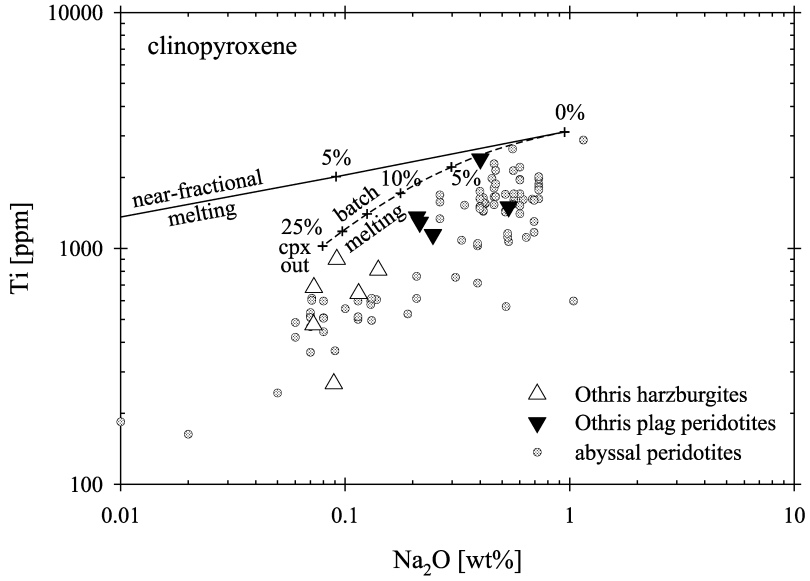

Fig. 11. Plot of Na_2O (wt %) vs Ti (ppm) in clinopyroxene. Continuous line: near-fractional melting at 0·1% increments. Dashed line: batch melting. Symbols and data sources as in Fig. 9.

plagioclase compositions. Calcic plagioclase has been observed in abyssal peridotites ($An_{91–96}$, Hamlyn & Bonatti, 1980) and in MORB ($An_{85–94}$; Donaldson & Brown, 1977; Stakes *et al.*, 1984; Price *et al.*, 1986; Natland, 1989; Sinton *et al.*, 1993). Melts with high Ca-number [100 × Ca/(Ca + Na)] and/or high Al-number [100 × Al/(Al + Si)] can crystallize highly calcic plagioclase (Panjasawatwong *et al.*, 1995). Magmas of appropriate compositions to crystallize these most calcic plagioclases are not known among MORB glasses, but they are sometimes found as melt inclusions in near-liquidus phenocrysts (Donaldson & Brown, 1977; Danyushevsky *et al.*, 1988; Natland, 1989; Sobolev & Shimizu, 1993). Near-fractional melting rapidly depletes the residue in Na_2O (Fig. 11), resulting in depleted melt increments with high Ca-number. These depleted melt increments, however, are rarely preserved because of effective mixing and homogenization of magmas in transit to, or within, sub-ridge magma chambers (Duncan & Green, 1980; Natland, 1989; Sobolev & Shimizu, 1993). The observed textures and mineral compositions of Othris plagioclase peridotites are therefore fully compatible with formation by a melt infiltration process in a MORB environment.

Clinopyroxene and plagioclase of the Othris plagioclase peridotites have more depleted LREE abundances than those inferred for these minerals in equilibrium with average N-MORB (Fig. 12). That is, the trapped melts from which clinopyroxene and plagioclase crystallized were depleted in incompatible trace elements. Calculations using the dry melting models show that the clinopyroxene REE compositions closely match those of clinopyroxene calculated to be in equilibrium with depleted melt increments produced by 4–9% multistage melting with 4% melting in the garnet stability field and 0–5% melting in the spinel stability field (Fig. 10). Similar depleted impregnating melts have been described in the Alpine–Apennine ophiolitic peridotites (Rampone *et al.*, 1997).

Whereas four out of the five plagioclase peridotites might be derived from 9% incremental melting with different degrees of melt–rock interaction (Fig. 12), sample GOF1 appears impregnated by an unrelated, more fertile (less depleted) melt. The near-fractional melting regime required to produce the depleted melt fractions is consistent with the melting process invoked to explain the primary residual compositions of the studied peridotites. The depleted melts, however, must have been derived from a source that was less depleted than the studied plagioclase-free peridotites from the Fournos Kaïtsa area, which were produced by ~15% near-fractional melting. Additionally, the observed disequilibrium between residual spinel and newly crystallized silicates indicates that the melts could not have been generated from a similar peridotite in the immediate vicinity (Allan & Dick, 1996). Thus, the plagioclase peridotites were impregnated by exotic melts derived from a deeper, only slightly depleted lherzolitic mantle source that was probably garnet bearing. Apparently, the impregnation by LREE-depleted, exotic melts is distinct from the melt percolation event recorded in the spinel harzburgites, which underwent selective enrichment in large

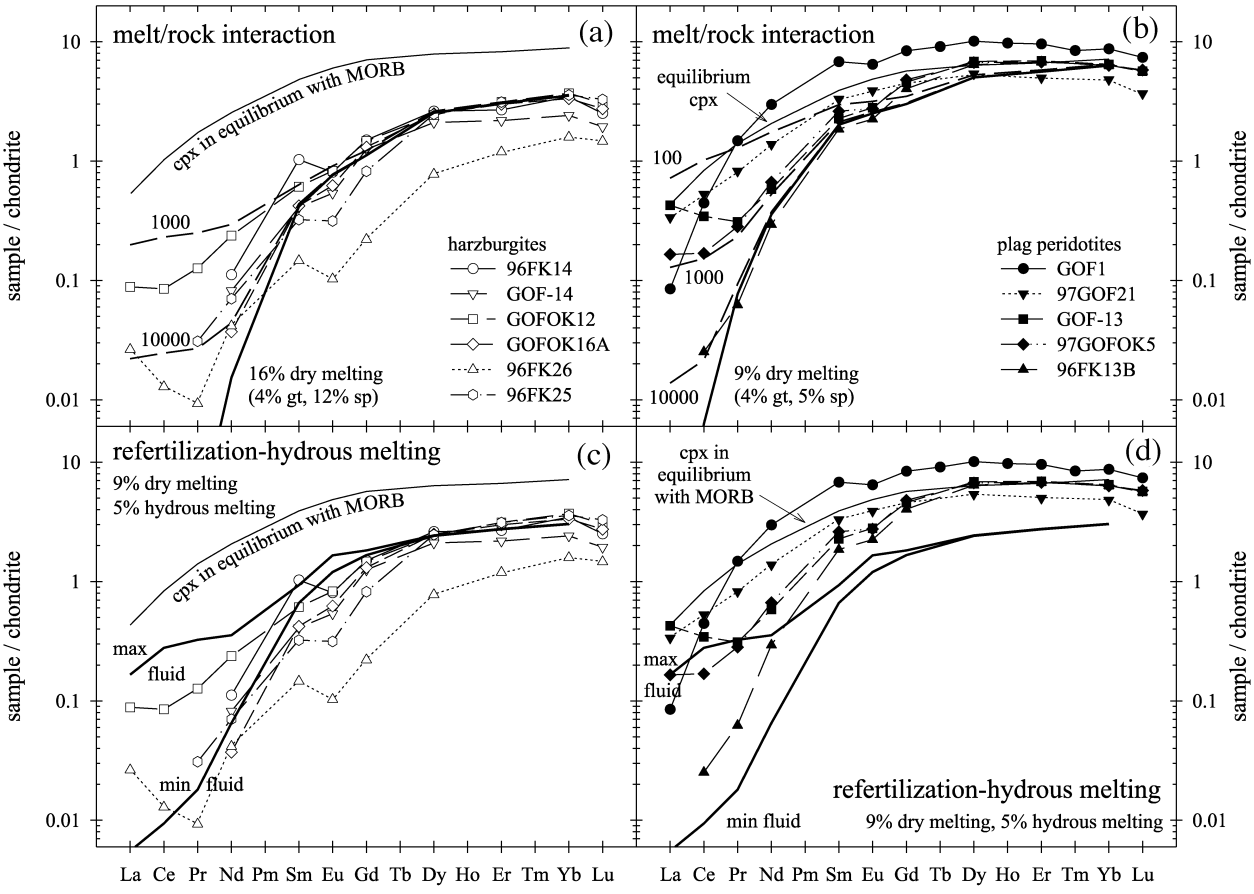

Fig. 12. Results of modelling the clinopyroxene compositions in the Othris peridotites in terms of dry partial melting followed by melt–rock interaction (a, b) and as refertilization–hydrous melting (c, d). Fine continuous lines represent clinopyroxene compositions in equilibrium with N-MORB (Sun & McDonough, 1989). The melt–rock interaction process (top) was modelled as proposed by Kelemen *et al.* (1990): ascending liquids from the deeper (more fertile) part of the mantle react with a depleted peridotite in shallower parts of the mantle. (a) Othris harzburgites: a 3% aggregate melt from the MORB source reacts with the residue of 16% melting (bold continuous line) shown in Fig. 10. Bold dashed lines show REE enrichment in clinopyroxene with peridotite/melt ratios of 1000 and 10 000. The reaction shown is for constant melt mass. (b) Othris plagioclase peridotites: a 3% aggregate melt from the MORB source reacts with the residue of 9% melting (bold continuous line) shown in Fig. 10. Bold dashed lines show REE enrichment in clinopyroxene with peridotite/melt ratios of 100, 1000 and 10 000. (c) and (d) refertilization–hydrous melting was modelled as suggested by Bizimis *et al.* (2000). The bold continuous lines are the limits of the model clinopyroxene compositions using the minimum (min) and maximum (max) concentrations in the fluid component, respectively (Table 9). Normalized as in Fig. 6.

ion lithophile elements and LREE. However, it cannot be excluded that the two processes were operated by the same percolation event under different physical conditions. The interaction of peridotite mantle with larger volumes of LREE-depleted melts led to the formation of plagioclase-bearing assemblages, whereas the migration of small volumes of more evolved melts resulted in slight and selective enrichment of more incompatible elements in refractory spinel harzburgites.

Clinopyroxene and plagioclase of the Othris plagioclase peridotites probably crystallized from rising late-stage melts (or later off-axis melts) entering the basal region of conductively cooled mantle lithosphere in a MOR setting rather than a back-arc or island-arc setting. Although the presence of H_2O in arc magmas can force crystallization of more calcic plagioclase than would crystallize from the same composition under anhydrous conditions (Arculus & Wills, 1980; Johannes, 1989; Sisson & Grove, 1993), the An difference between hydrous and anhydrous magmas decreases for very high melt Ca-number (Panjasawatwong *et al.*, 1995). Unless the magma was very hydrous ($\sim$6 wt % H_2O), the magma must have had abnormally high Ca-number to crystallize the calcic plagioclases found in the Othris plagioclase peridotites (Panjasawatwong *et al.*, 1995). High water contents, however, markedly suppress the crystallization of

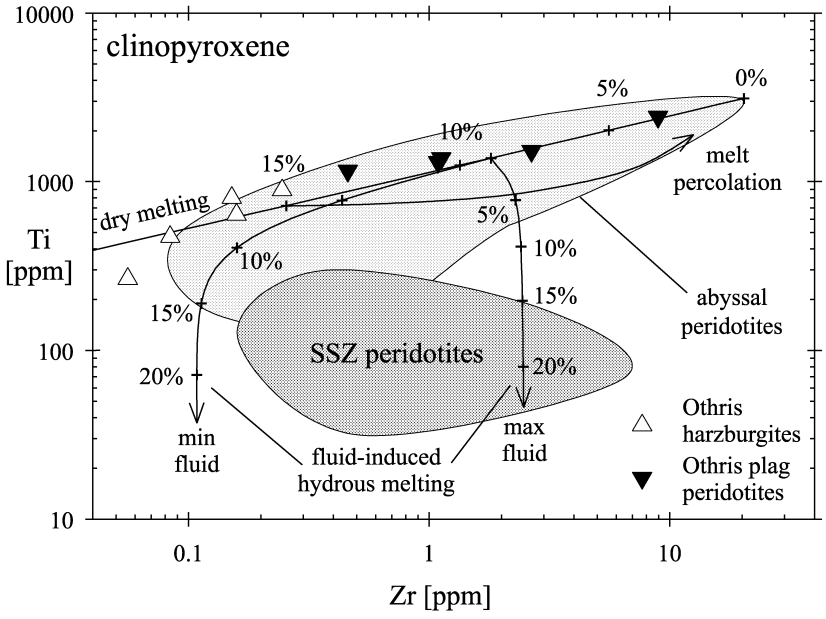

Fig. 13. Plot of Ti vs Zr (in ppm) in clinopyroxene. Three processes are shown: dry melting, melt percolation, and fluid-induced hydrous melting. Numbers along the line are percent melting. (See text for details.)

plagioclase (e.g. Green, 1982). For most arc magmas, there is abundant evidence of extended clinopyroxene crystallization before plagioclase appearance (e.g. Barsdell, 1988). As the boninitic and komatiitic lavas, which also occur in the Lamia outcrops of the Othris Ophiolite, contain olivine and clinopyroxene phenocrysts but no plagioclase phenocrysts (Cameron *et al.*, 1979; Paraskevopoulos & Economou, 1986; Economou-Eliopoulos & Paraskevopoulos, 1989), these lavas do not appear related to the melt impregnation event.

Based on the calculated trace element composition of a melt in equilibrium with clinopyroxene in the plagioclase peridotites, the inferred impregnating melt can be shown not to be of an island-arc origin. That is, melts in equilibrium with Othris clinopyroxenes do not show LREE and Sr enrichment nor high field strength element depletions (Nb and Ta) typical for island-arc basalts and boninites. In addition, melts derived from a depleted mantle wedge in a supra-subduction zone setting are unlikely to have high enough Ti and HREE contents to crystallize the trace element contents observed in clinopyroxene and plagioclase in the Othris plagioclase peridotites (Fig. 9). Although the refertilization–hydrous melting model can explain the comparatively low HREE contents of orthopyroxene from Eretria (Bizimis *et al.*, 2000), it fails to reproduce the high Ti and HREE contents of clinopyroxene in the plagioclase peridotites from Fournos Kaïtsa (Figs 12 and 13).

Furthermore, it can be shown that the peridotites were unrelated to the boninites and komatiites before melt impregnation. Spinels in boninites and komatiites found in the Othris Ophiolite are characterized by exceptionally high Cr-number = 65–85 (Cameron *et al.*, 1979; Paraskevopoulos & Economou, 1986; Economou-Eliopoulos & Paraskevopoulos, 1989), typical of boninites and komatiites world-wide [see compilation by Barnes & Roeder (2001)]. In contrast to the much more refractory spinels formed by hydrous melting in a supra-subduction zone setting with Cr-number >60 (Dick & Bullen, 1984; Barnes & Roeder, 2001), spinels in the plagioclase peridotites (Cr-number 30–35) fall into the MORB field.

Geological implications

The peridotites from the Fournos Kaïtsa area record moderate degrees of partial melting, melt extraction and melt migration followed by impregnation by a late-stage or second-stage melt. This evolution is similar to that observed in slow-spreading mid-ocean ridges (e.g. Dick, 1989; Johnson *et al.*, 1990). The melts that impregnated the plagioclase peridotites were derived from more fertile peridotites forming deeper mantle levels than the depleted harzburgites cropping out in the Fournos Kaïtsa block. Because of their origin as refertilization products, the presence of plagioclase peridotites in Othris cannot be used to infer low degrees of partial melting (see Nicolas, 1989) and

hence formation of the ophiolite during the initial stage of rifting (see Menzies & Allen, 1974).

This study of the Fournos Kaïtsa area establishes that the spinel harzburgites are comparable with 'typical' residua formed beneath moderate to slow-spreading ridges. Although an episode of hydrous melting cannot be ruled out for the initial depletion of the Othris peridotites, subduction-related processes are not necessary for the petrogenesis of the spinel harzburgites and the plagioclase peridotites in the Fournos Kaïtsa area. A slow-spreading mid-ocean ridge environment is therefore the favoured tectonic setting for the Othris Ophiolite, in agreement with previous suggestions based on the distribution of immobile trace elements in the mafic rocks (Bickle & Nisbet, 1972; Pearce *et al.*, 1984).

The presence of boninitic and komatiitic lavas in the Agrilia Formation (Fig. 1, 10 km NE of Lamia; Cameron *et al.*, 1979; Paraskevopoulos & Economou, 1986; Economou-Eliopoulos & Paraskevopoulos, 1989) and of highly depleted clinopyroxene-free harzburgite in Eretria (Fig. 1, 45 km east of the Fournos Kaïtsa area; Bizimis *et al.*, 2000) points to a subduction zone component in other parts of the Othris Ophiolite. Thus, the Othris Ophiolite as a whole appears to contain evidence of more than one mantle source and possibly more than one tectonic setting. Two different mantle sources have also been proposed for the Pindos ophiolite complex in the NW of Othris (Pearce *et al.*, 1984), because of the presence of lavas ranging from MORB to boninite affinities (Capedri *et al.*, 1980).

The temporal and spatial relation of the MORB and subduction zone component cannot be resolved from our study. Economou-Eliopoulos & Paraskevopoulos (1989) considered the occurrence of boninitic and komatiitic lavas in the Agrilia Formation as older than the ophiolite complex representing MOR-type spreading (the Mirna group; Smith *et al.*, 1975), thus concluding that the subduction zone component decreased over time. In contrast, Smith (1979, 1993) argued that the Pindos, Vourinos, and Othris ophiolites belonged to the same tectonic unit, which originated by spreading and later convergence. In analogy with Pindos, a subduction zone component may have been introduced in Othris and its magnitude may have increased over time (Pearce *et al.*, 1984; Smith, 1993). Clearly, a deeper evaluation of the conflicting views outlined above requires a more precise assessment of the tectonic setting of the Greek ophiolites. The combination of detailed structural, petrological, and geochemical investigations reported here establishes that part of the Othris complex was formed at a 'typical' MOR. Similar detailed work is required in other parts of the ophiolite belt to establish the relationships between the inferred MORB, komatiite, and SSZ volcanism.

ACKNOWLEDGEMENTS

We would like to acknowledge T. Bouten and H. L. M. van Roermund for help with the microprobe work. Careful reviews by Yaoling Niu, Elisabetta Rampone, Vincent Salters, and Riccardo Vannucci helped to improve the manuscript. Marjorie Wilson is thanked for her highly constructive editorial handling.

REFERENCES

Allan, J. F. & Dick, H. J. B. (1996). Cr-rich spinel as a tracer for melt migration and melt–wall rock interaction in the mantle: Hess Deep, leg 147. In: Mével, C., Gillis, K. M., Allan, J. F. & Meyer, P. S. (eds) *Proceedings of the Ocean Drilling Program: Scientific Results, 147*. College Station, TX: Ocean Drilling Program, pp. 157–172.

Arculus, R. J. & Wills, K. J. A. (1980). The petrology of plutonic blocks and inclusions from the Lesser Antilles island arc. *Journal of Petrology* **21**, 143–168.

Asimow, P. D. (1999). A model that reconciles major- and trace-element data from abyssal peridotites. *Earth and Planetary Science Letters* **169**, 303–319.

Asimow, P. D. & Stolper, E. M. (1999). Steady-state mantle–melt interactions in one dimension: I. Equilibrium transport and melt focusing. *Journal of Petrology* **40**, 475–494.

Baker, M. B. & Beckett, J. R. (1999). The origin of abyssal peridotites: a reinterpretation of constraints based on primary bulk compositions. *Earth and Planetary Science Letters* **171**, 49–61.

Baker, M. B. & Stolper, E. M. (1994). Determining the composition of high-pressure mantle melts using diamond aggregates. *Geochimica et Cosmochimica Acta* **58**, 2811–2827.

Barnes, S. J. & Roeder, P. L. (2001). The range of spinel compositions in terrestrial mafic and ultramafic rocks. *Journal of Petrology* **42**, 2279–2302.

Barsdell, M. (1988). Petrology and petrogenesis of clinopyroxene-rich tholeiitic lavas. Merelava Volcano, Vanuata. *Journal of Petrology* **29**, 927–964.

Batanova, V. G., Sobolev, A. V. & Schmincke, H.-U. (1994). Mantle lherzolites from Troodos ophiolites: mineralogy and ion probe geochemistry of clinopyroxenes. *Mineralogical Magazine* **58A**, 57–58.

Batanova, V. G., Suhr, G. & Sobolev, A. V. (1998). Origin of geochemical heterogeneity in the mantle peridotites from the Bay of Islands Ophiolite, Newfoundland, Canada: ion probe study of clinopyroxenes. *Geochimica et Cosmochimica Acta* **62**, 853–866.

Bickle, M. J. & Nisbet, E. G. (1972). The oceanic affinities of some alpine mafic rocks based on their Ti–Zr–Y contents. *Journal of the Geological Society, London* **128**, 267–271.

Bizimis, M., Salters, V. J. M. & Bonatti, E. (2000). Trace and REE content of clinopyroxenes from supra-subduction zone peridotites. Implications for melting and enrichment processes in island arcs. *Chemical Geology* **165**, 67–85.

Bodinier, J. L., Vasseur, G., Vernieres, J., Dupuy, C. & Fabriès, J. (1990). Mechanisms of mantle metasomatism: geochemical evidence from the Lherz orogenic peridotite. *Journal of Petrology* **31**, 597–628.

Boudier, F. & Nicolas, A. (1985). Harzburgite and lherzolite subtypes in ophiolitic and oceanic enivronments. *Earth and Planetary Science Letters* **76**, 84–92.

Boynton, W. V. (1984). Cosmochemistry of the REE: meteorite studies. In: Henderson, P. (ed.) *REE Geochemistry. Developments in Geochemistry 2*. Amsterdam: Elsevier, pp. 63–114.

Cameron, W. E., Nisbet, E. G. & Dietrich, V. J. (1979). Boninites, komatiites and ophiolitic basalts. *Nature* **280**, 550–553.

Cannat, M., Bideau, D. & Hébert, R. (1990). Plastic deformation and magmatic impregnation in serpentinized ultramafic rocks from the Garret transform fault (East Pacific Rise). *Earth and Planetary Science Letters* **101**, 216–232.

Capedri, S., Venturelli, G., Bocchi, G., Dostal, J., Garuti, G. & Rossi, A. (1980). The geochemistry and petrogenesis of an ophiolitic sequence from Pindos, Greece. *Contributions to Mineralogy and Petrology* **74**, 189–200.

Danyushevsky, L. V., Sobolev, A. V. & Dmitriev, L. V. (1988). Orthopyroxene-bearing low-Ti tholeiites—the new type of oceanic ridge tholeiite. *Doklady Akademii Nauk SSSR* **292**, 102–105.

DePaolo, D. (1981). Trace element and isotopic effects of combined wallrock assimilation and fractional crystallization. *Earth and Planetary Science Letters* **53**, 189–202.

Dick, H. J. B. (1989). Abyssal peridotites, very slow spreading ridges and ocean ridge magmatism. In: Saunders, A. D. & Norry, M. J. (eds) *Magmatism in the Ocean Basins*. *Geological Society, London, Special Publications* **42**, 71–105.

Dick, H. J. B. & Bullen, T. (1984). Chromian spinel as a petrogenetic indicator in abyssal and alpine-type peridotites and spatially associated lavas. *Contributions to Mineralogy and Petrology* **86**, 54–76.

Dick, H. J. B. & Natland, J. H. (1996). Late-stage melt evolution and transport in the shallow mantle beneath the East Pacific Rise. In: Mével, C., Gillis, K. M., Allan, J. F. & Meyer, P. S. (eds) *Proceedings of the Ocean Drilling Program: Scientific Results, 147*. College Station, TX: Ocean Drilling Program, pp. 103–134.

Dijkstra, A., Drury, M. R. & Vissers, R. L. M. (2001). Structural petrology of plagioclase peridotites in the West Othris Mountains (Greece): melt impregnation in mantle lithosphere. *Journal of Petrology* **42**, 5–24.

Dijkstra, A. H., Drury, M. R., Vissers, R. L. M. & Newman, J. (2002). On the role of melt–rock reaction in mantle shear zone formation in the Othris Peridotite Massif (Greece). *Journal of Structural Geology* **24**, 1431–1450.

Dijkstra, A. H., Barth, M., Drury, M. R., Mason, P. R. D. & Vissers, R. L. M. (2003). Diffuse porous flow and melt–rock reaction in the lithosphere at a slow-spreading ridge: a structural petrology and LA–ICP-MS study of the Othris peridotite massif (Greece). *Geochemistry, Geophysics, Geosystems* (in press).

Donaldson, C. H. & Brown, R. W. (1977). Refractory megacrysts and magnesium-rich melt inclusions within spinel in oceanic tholeiites: indicators of magma mixing and parental magma composition. *Earth and Planetary Science Letters* **37**, 81–89.

Duncan, R. A. & Green, D. H. (1980). Role of multistage melting in the formation of oceanic crust. *Geology* **8**, 22–26.

Duncan, R. A. & Green, D. H. (1987). The genesis of refractory melts in the formation of oceanic crust. *Contributions to Mineralogy and Petrology* **96**, 326–342.

Economou-Eliopoulos, M. & Parakevopoulos, G. M. (1989). Platinum-group elements and gold in komatiitic rocks from the Agrilia Formation, Othrys ophiolite complex, Greece. *Chemical Geology* **77**, 149–158.

Eggins, S. M., Rudnick, R. L. & McDonough, W. F. (1998). The composition of peridotites and their minerals: a laser ablation ICP-MS study. *Earth and Planetary Science Letters* **154**, 53–71.

Elthon, D. (1992). Chemical trends in abyssal peridotites: re-fertilization of depleted suboceanic mantle. *Journal of Geophysical Research* **97**, 9015–9025.

Engi, M. & Evans, B. W. (1980). A re-evaluation of the olivine–spinel geothermometer: discussion. *Contributions to Mineralogy and Petrology* **73**, 201–203.

Green, T. H. (1982). Anatexis of mafic crust and high pressure crystallization of andesite. In: Thorpe, R. S. (ed.) *Andesites: Orogenic Andesites and Related Rocks*. Chichester: Wiley, pp. 465–487.

Günther, D., Frischknecht, R., Heinrich, C. A. & Kahlert, H.-J. (1997). Capabilities of an argon fluoride 193 nm excimer laser for laser ablation inductively coupled plasma mass spectrometry microanalysis of geological materials. *Journal of Analytical Atomic Spectrometry* **12**, 939–944.

Hamlyn, P. R. & Bonatti, E. (1980). Petrology of mantle-derived ultramafics from the Owen Fracture Zone, northwest Indian Ocean: implications for the nature of the oceanic upper mantle. *Earth and Planetary Science Letters* **48**, 65–79.

Hellebrand, E., Snow, J. E., Dick, H. J. B. & Hofmann, A. W. (2001). Coupled major and trace elements as indicators of the extent of melting in mid-ocean-ridge peridotites. *Nature* **410**, 677–681.

Hynes, A. (1974). Igneous activity at the birth of an ocean basin in eastern Greece. *Canadian Journal of Earth Sciences* **11**, 842–853.

Johannes, W. (1989). Melting of plagioclase–quartz assemblages at 2 kbar water pressure. *Contributions to Mineralogy and Petrology* **103**, 270–276.

Johnson, K. T. M. (1998). Experimental determination of partition coefficients for rare earth and high-field-strength elements between clinopyroxene, garnet, and basaltic melt at high pressures. *Contributions to Mineralogy and Petrology* **133**, 60–68.

Johnson, K. T. M. & Dick, H. J. B. (1992). Open system melting and temporal and spatial variation of peridotite and basalt at the Atlantis II fracture zone. *Journal of Geophysical Research* **97**, 9219–9241.

Johnson, K. T., Dick, H. J. B. & Shimizu, N. (1990). Melting in the oceanic upper mantle: an ion microprobe study of diopsides in abyssal peridotites. *Journal of Geophysical Research* **95**, 2661–2678.

Jones, G. & Robertson, A. H. F. (1991). Tectono-stratigraphy and evolution of the Mesozoic Pindos ophiolite and related units, Northwestern Greece. *Journal of the Geological Society, London* **148**, 267–288.

Kelemen, P. B., Johnson, K. T. M., Kinzler, R. J. & Irving, A. J. (1990). High-field-strength element depletions in arc basalts due to mantle–magma interaction. *Nature* **345**, 521–524.

Kelemen, P. B., Dick, H. J. B. & Quick, J. E. (1992). Production of harzburgite by pervasive melt–rock reaction in the upper mantle. *Nature* **358**, 635–641.

Kelemen, P. B., Shimizu, N. & Dunn, T. (1993). Relative depletion of niobium in some arc magmas and the continental crust: partitioning of K, Nb, La and Ce during melt/rock reaction in the upper mantle. *Earth and Planetary Science Letters* **120**, 111–134.

Kelemen, P. B., Shimizu, N. & Salters, V. J. M. (1995*a*). Extraction of mid-ocean-ridge basalt from the upwelling mantle by focused flow of melt in dunite channels. *Nature* **375**, 747–753.

Kelemen, P. B., Whitehead, J. A., Aharonov, E. & Jordahl, K. A. (1995*b*). Experiments on flow focusing in soluble porous media, with application to melt extraction from the mantle. *Journal of Geophysical Research* **100**, 475–496.

Kelemen, P. B., Hirth, G., Shimizu, N., Spiegelman, M. & Dick, H. J. B. (1997). A review of melt migration processes in the adiabatically upwelling mantle beneath oceanic spreading ridges. *Philosophical Transactions of the Royal Society of London, Series A* **355**, 283–318.

Longerich, H. P., Jackson, S. E. & Günther, D. (1996). Laser ablation inductively coupled plasma mass spectrometric transient signal data acquisition and analyte concentration calculation. *Journal of Analytical Atomic Spectrometry* **11**, 899–904.

Menzies, M. (1973). Mineralogy and partial melt textures within an ultramafic–mafic body, Greece. *Contributions to Mineralogy and Petrology* **42**, 273–285.

Menzies, M. (1975). Spinel compositional variation in the crustal and mantle lithologies of the Othris ophiolite. *Contributions to Mineralogy and Petrology* **51**, 303–309.

Menzies, M. (1976). Rare earth geochemistry of fused ophiolitic and alpine lherzolites—I. Othris, Lanzo and Troodos. *Geochimica et Cosmochimica Acta* **40**, 645–656.

Menzies, M. & Allen, C. (1974). Plagioclase lherzolite–residual mantle relationships within two eastern Mediterranean ophiolites. *Contributions to Mineralogy and Petrology* **45**, 197–213.

Miyashiro, A. (1973). The Troodos ophiolitic complex was probably formed in an island arc. *Earth and Planetary Science Letters* **19**, 218–224.

Moores, E. M., Kellogg, L. H. & Dilek, Y. (2000). Tethyan ophiolites, mantle convection, and tectonic 'historical contingency': a resolution of the 'ophiolite conundrum'. In: Dilek, Y., Moores, E. M., Elthon, D. & Nicolas, A. (eds) *Ophiolites and Oceanic Crust: New Insights from Field Studies and the Ocean Drilling Program. Geological Society of America, Special Papers* **349**, 3–12.

Nagata, J., Goto, A. & Obata, M. (1983). The parabolic pattern of chromium partitioning observed between pyroxenes and spinel from ultramafic rocks and its petrological significance. *Contributions to Mineralogy and Petrology* **82**, 42–51.

Natland, J. H. (1989). Partial melting of a lithologically heterogeneous mantle—inferences from crystallization histories of magnesian abyssal tholeiites from the Siqueiros Fracture Zone. In: Saunders, A. D. & Norry, M. J. (eds) *Magmatism in the Ocean Basins. Geological Society, London, Special Publications* **42**, 41–70.

Navon, O. & Stolper, E. (1987). Geochemical consequences of melt percolation: the upper mantle as a chromatographic column. *Journal of Geology* **95**, 285–308.

Nicolas, A. (1986). Structure and petrology of peridotites: clues to their geodynamic environment. *Reviews of Geophysics* **24**, 875–895.

Nicolas, A. (1989). *Structures of Ophiolites and Dynamics of Oceanic Lithosphere*. Dordrecht: Kluwer Academic.

Nicolas, A. & Dupuy, C. (1984). Origin of ophiolitic and oceanic lherzolites. *Tectonophysics* **110**, 177–187.

Niu, Y. (1997). Mantle melting and melt extraction processes beneath ocean ridges: evidence from abyssal peridotites. *Journal of Petrology* **38**, 1047–1074.

Niu, Y. & Hékinian, R. (1997). Spreading-rate dependence of the extent of mantle melting beneath ocean ridges. *Nature* **385**, 326–329.

Niu, Y., Langmuir, C. H. & Kinzler, R. J. (1997). The origin of abyssal peridotites: a new perspective. *Earth and Planetary Science Letters* **152**, 251–265.

Obata, M. & Nagahara, N. (1987). Layering of alpine-type peridotite and the segregation of partial melt in the upper mantle. *Journal of Geophysical Research* **92**, 3467–3474.

Panjasawatwong, Y., Danyushevsky, L. V., Crawford, A. J. & Harris, K. L. (1995). An experimental study of the effects of melt composition on plagioclase–melt equilibria at 5 and 10 kbar: implications for the origin of magmatic high-An plagioclase. *Contributions to Mineralogy and Petrology* **118**, 420–432.

Paraskevopoulos, G. M. & Economou, M. I. (1986). Komatiite-type ultramafic lavas from the Agrilia Formation, Othrys Ophiolite complex, Greece. *Ofioliti* **11**, 293–304.

Parkinson, I. J., Pearce, J. A., Thirlwall, M. F., Johnson, K. T. M. & Ingram, G. (1992). Trace element geochemistry of peridotites from the Izu–Bonin–Mariana forearc, Leg 125. In: Fryer, P., Pearce, J. A. & Stokking, L. B. (eds) *Proceedings of the Ocean Drilling Program: Scientific Results, 125*. College Station, TX: Ocean Drilling Program, pp. 487–506.

Pearce, J. A., Lippard, S. J. & Roberts, S. (1984). Characteristics and tectonic significance of supra-subduction zone ophiolites. In: Kokelaar, P. B. & Howells, M. F. (eds) *Marginal Basin Geology. Geological Society, London, Special Publications* **16**, 77–94.

Pearce, N. J. G., Perkins, W. T., Westgate, J. A., Gorton, M. P., Jackson, S. E., Neal, C. R. & Chenery, S. P. (1997). A compilation of new and published major and trace element data for NIST SRM 610 and NIST SRM 612 glass reference materials. *Geostandards Newsletter* **21**, 115–144.

Price, R. C., Kennedy, A. K., Riggs-Sneeringer, M. & Frey, F. A. (1986). Geochemistry of basalts from the Indian Ocean triple junction: implications for the generation and evolution of Indian Ocean ridge basalts. *Earth and Planetary Science Letters* **78**, 379–396.

Quick, J. E. (1981). Petrology and petrogenesis of the Trinity peridotite, an upper mantle diapir in the eastern Klamath Mountains, northern California. *Journal of Geophysical Research* **86**, 11837–11863.

Rampone, E. & Piccardo, G. B. (2000). The ophiolite–oceanic lithosphere analogue: new insights from the Northern Apennines (Italy). In: Dilek, Y., Moores, E. M., Elthon, D. & Nicolas, A. (eds) *Ophiolites and Oceanic Crust: New Insights from Field Studies and the Ocean Drilling Program. Geological Society of America, Special Papers* **349**, 21–34.

Rampone, E., Piccardo, G. B., Vannucci, R., Bottazzi, P. & Ottolini, L. (1993). Subsolidus reactions monitored by trace element partitioning: the spinel- to plagioclase-facies transition in mantle peridotites. *Contributions to Mineralogy and Petrology* **115**, 1–17.

Rampone, E., Hofmann, A. W., Piccardo, G. B., Vannucci, R., Bottazzi, P. & Ottolini, L. (1995). Petrology, mineral, and isotope geochemistry of the External Liguride peridotites (Northern Apennine, Italy). *Journal of Petrology* **36**, 81–105.

Rampone, E., Piccardo, G. B., Vannucci, R. & Bottazzi, P. (1997). Chemistry and origin of trapped melts in ophiolitic peridotites. *Geochimica et Cosmochimica Acta* **61**, 4557–4569.

Rassios, A. & Konstantopoulou, G. (1993). Emplacement tectonism and the position of chrome ores in the Mega Isoma peridotites, SW Othris, Greece. *Bulletin of the Geological Society of Greece* **28**, 463–474.

Rassios, A. & Smith, A. G. (2001). Constraints on the formation and emplacement age of western Greek ophiolites (Vourinos, Pindos, and Othris) inferred from deformation structures in peridotites. In: Dilek, Y., Moores, E., Elthon, D. & Nicolas, A. (eds) *Ophiolites and Oceanic Crust: New Insights from Field Studies and the Ocean Drilling Program. Geological Society of America, Special Papers* **349**, 473–484.

Rassios, A., Grivas, E. & Vacondios, I. (1999). The structural–geochemical–metallogenetic unification of the Pindos and Vourinos Ophiolites. *Journal of Conference Abstracts* **4**, 407.

Robertson, A. H. F., Clift, P. D., Degnan, P. J. & Jones, G. (1991). Palaeogeographic and palaeotectonic evolution of the Eastern

Mediterranean Neotethys. *Palaeogeography, Palaeoclimatology, Palaeoecology* **87**, 289–343.

Roeder, P. L., Campbell, I. H. & Jamieson, H. E. (1979). A re-evaluation of the olivine–spinel geothermometer. *Contributions to Mineralogy and Petrology* **68**, 325–334.

Ross, K. & Elthon, D. (1993). Cumulates from strongly depleted mid-ocean-ridge basalt. *Nature* **365**, 826–829.

Ross, K. & Elthon, D. (1997). Extreme incompatible trace-element depletion of diopside in residual mantle from south of the Kane Fracture Zone. In: Karson, J. A., Cannat, M., Miller, D. J. & Elthon, D. (eds) *Proceedings of the Ocean Drilling Program: Scientific Results, 153.* College Station, TX: Ocean Drilling Program, pp. 277–284.

Seyler, M. & Bonatti, E. (1997). Regional-scale melt–rock interaction in lherzolitic mantle in the Romanche Fracture Zone (Atlantic Ocean). *Earth and Planetary Science Letters* **146**, 273–287.

Shaw, D. M. (1970). Trace element fractionation during anatexis. *Geochimica et Cosmochimica Acta* **34**, 237–243.

Sinton, C. W., Christie, D. M., Coombs, V. L., Nielsen, R. L. & Fisk, M. R. (1993). Near primary melt inclusions in anorthite phenocrysts from the Galapagos Platform. *Earth and Planetary Science Letters* **119**, 527–537.

Sisson, T. W. & Grove, T. L. (1993). Experimental investigations of the role of H_2O in calc-alkaline differentiation and subduction zone magmatism. *Contributions to Mineralogy and Petrology* **113**, 143–166.

Smith, A. G. (1979). Othris, Pindos and Vourinos ophiolites and the Pelagonian zone. *6th Colloquium on the Geology of the Aegean Region, Athens, Greece*. Institute of Geological and Mining Research: Athens, pp. 1369–1374.

Smith, A. G. (1993). Tectonic significance of the Hellenic–Dinaric ophiolites. In: Prichard, H. M., Alabaster, T., Harris, N. B. W. & Neary, C. R. (eds) *Magmatic Processes and Plate Tectonics. Geological Society, London, Special Publications* **76**, 213–243.

Smith, A. G. & Spray, J. G. (1984). A half-ridge transform model for the Hellenic–Dinaric ophiolites. In: Dixon, J. E. & Robertson, A. H. F. (eds) *The Geological Evolution of the Eastern Mediterranean. Geological Society, London, Special Publications* **17**, 629–644.

Smith, A. G., Hynes, A. J., Menzies, M., Nisbet, E. G., Price, I., Welland, M. J. & Ferrière, J. (1975). The stratigraphy of the Othris Mountains, eastern central Greece: a deformed Mesozoic continental margin sequence. *Eclogae Geologicae Helveticae* **68**, 463–481.

Sobolev, A. V. & Shimizu, N. (1993). Ultra-depleted primary melt included in an olivine from the mid-Atlantic ridge. *Nature* **363**, 151–154.

Stampfli, G. M., Mosar, J., De Bono, A. & Vavasi, I. (1998). Late Paleozoic, early Mesozoic plate tectonics of the Western Tethys. *Bulletin of the Geological Society of Greece* **XXXII**, 113–120.

Stakes, D. S., Shervais, J. W. & Hopson, C. A. (1984). The volcanic–tectonic cycle of the FAMOUS and AMAR Valleys, mid-Atlantic Ridge (36°47′N): evidence from basalt glass and phenocryst compositional variations for a steady state magma chamber beneath the valley midsection. *Journal of Geophysical Research* **89**, 6995–7028.

Sun, S.-S. & McDonough, W. F. (1989). Chemical and isotopic systematics of ocean basalts: implications for mantle composition and processes. In: Saunders, A. D. & Norry, M. J. (eds) *Magmatism in the Ocean Basins. Geological Society, London, Special Publications* **42**, 313–345.

Takazawa, E., Frey, F. A., Shimizu, N., Obata, M. & Bodinier, J. L. (1992). Geochemical evidence for melt migration and reaction in the upper mantle. *Nature* **359**, 55–58.

Takazawa, E., Frey, F., Shimizu, N. & Obata, M. (1996). Evolution of the Horoman Peridotite (Hokkaido, Japan): implications from pyroxene compositions. *Chemical Geology* **134**, 3–26.

Takazawa, E., Frey, F. A., Shimizu, N. & Obata, M. (2000). Whole rock compositional variations in an upper mantle peridotite (Horoman, Hokkaido, Japan): are they consistent with a partial melting process? *Geochimica et Cosmochimica Acta* **64**, 695–716.

Tartarotti, P., Susini, S., Nimis, P. & Ottolini, L. (2002). Melt migration in the upper mantle along the Romanche Fracture Zone (Equatorial Atlantic). *Lithos* **63**, 125–149.

Walter, M. J. (1998). Melting of garnet peridotite and the origin of komatiite and depleted lithosphere. *Journal of Petrology* **39**, 29–60.